Mechanical Properties of an Exhumed Cast Iron Pipe Material

By

Ismail Ali

A thesis submitted to the School of Graduate Studies

in partial fulfillment of the requirements for the degree of

Master of Engineering

Department of Civil Engineering

Faculty of Engineering and Applied Science

Memorial University of Newfoundland

May - 2017

St. John’s Newfoundland and Labrador Canada

Abstract

Cast iron is one of the most commonly used materials for municipal water mains. Although cast iron pipes are no longer used for new water mains, a significant portion of existing water mains are still cast iron. These aged cast iron pipes are undergoing deterioration and are susceptible to leakage and breakage. In this thesis, a deteriorating cast water main is investigated to understand the failure mechanism and to determine the mechanical properties of the material as a tool for the structural integrity assessment of existing pipes. A better understanding of pipe failure mechanisms can lead to a realistic evaluation of the strength of the pipes in the system, and hence of their current level of safety.

A pipe segment exhumed after failure from the city of Mount Pearl in the province of Newfoundland and Labrador is investigated. The failure is apparently due to subcritical corrosion fatigue crack growth. Localized defects were observed over the pipe wall thickness through which water could penetrate, providing an environment conducive to stress corrosion cracking. Tensile tests were conducted at different rates of loading to examine the effects of loading rate. The ultimate tensile strengths of the specimens varied from around 150 MPa to around 200 MPa, which are independent of the rate of loading. However, the stress strain responses are dependent on the rate of loading. The Poisson's ratio of the material is determined through the measurement of longitudinal and lateral strains. Single Edge Notch Beam (SENB) tests are conducted to examine the mechanical properties in bending and to determine the fracture toughness. Numerical analyses using the finite element method (FEM) conducted to evaluate the performance of determined mechanical parameters in simulating the test conditions.

Acknowledgements

First and foremost, I would like to express my deepest gratitude and thanks to my supervisor, Dr. Ashutosh Sutra Dhar, for his optimism, guidance, patience, and his continued support and confidence in my efforts, which have always encouraged me to succeed in my studies. I have benefitted greatly from his experience in the field of my research.

I am thankful to the staff and technicians at Memorial University of Newfoundland, who have helped me during my research. I am also very grateful to my classmates and friends who have assisted me and given me advice during my programs.

Looking back over the past two years, I can think of many people who deserve credit for their contributions to my studies. Last, but not least, I would like to thank my family: my parents, brothers, sisters and close friends, for encouraging and supporting me throughout my graduate studies**.**

Table of Contents

List of Symbols and Acronyms

All symbols and acronyms used in this research are written below, even though they might also be explained throughout the text. For every parameter, metric units are used, though other units are also employed intermittently in the text. Unitless parameters are indicated by a symbol.

E_i =Initial Tangent Modulus [MPa]

E_s = Secant Modulus [MPa]

σ_u= Ultimate Tensile Strength [MPa]

ε_u= Ultimate Strains [-]

K_C= Fracture Toughness N/$mm^{3/2}$

S= Clear span of the Specimen [mm]

B= Thickness of the Specimen [mm]

w= Depth of the Specimen [mm]

a= Crack Length of the V notch [mm]

σ_{ys} = Cross-Sectional Tensile or Compressive stress [MPa]

M = Applied Bending Moment [N.mm]

Y = Distance from the centroidal axis to the point where the stress is calculated [mm]

I = Moment of Inertia of the Cross-Section [mm^4]

P = Total Applied Force [N]

L = Length of specimen (distance between supports) [mm]

b =Thickness of the Specimen [mm]

W =Width of the Specimen [mm]

$\left(\frac{P}{\Delta center}\right)$= Slope of the initial tangent line to the load-displacement curve [N/mm]

LVDT = Linear Voltage Displacement Transducer

ASA = American Statistical Association

ASTM =American Society for Testing and Materials

CSCE = Canadian Society of Civil Engineering

AWWA = American Water Works Association

PVC = Polyvinyl Chloride

SENB = Single-Edge Notched Bend

HR = Rockwell Hardness measurements

FEM = Finite Element Method

CI = Cast Iron

CF = Corrosion Fatigue

List of Tables

List of Figures

Chapter 1: Introduction and Overview

1.1 General

Since the beginning of civilization, the provision of a sufficient quantity of high quality water to human inhabitants has been a major concern. During ancient times, aqueducts were built to transport water from distant sources to central locations where the local supply of water was insufficient. In the middle of the seventeenth century, different materials such as wood, clay, and lead were used to make pipes for transporting water. The pipes were generally laid on a hydraulic grade line; however, these pipes were unable to resist high stresses. The evolution of cast iron pipes and the gradual decrease in their cost, together with the development of improved pumps driven by steam made it possible to connect public supplies and transport water to residents (McGhee 1991). This led to the wide usage of cast iron pipes from the end of the eighteenth century until the late 1960s, when ductile iron pipes began to be manufactured. Lately, plastic pipes (Polyvinyl chloride or PVC) have been produced and are popularly used for this type of application.

Many enhancements have been made with respect to the technology used to manufacture cast iron pipes, with the most rapid progress occurring with the changeover from the pit cast method to the centrifugally (spun) cast one. The mechanical properties of the cast iron material were influenced by the manufacturing method as well as mineralogy. The manufacturing methods and mineralogy of cast iron pipe materials are briefly outlined below.

1.2 Manufacturing of Cast Iron Pipes

The Handbook of Cast Iron Pipe (CIPRA, 1967) explains the manufacturing method of cast iron pipes. In the early 1920s, dry sand moulds (CSCE, 1916) were used to produce the pipes. Pipes called McWane pipes, (Babbitt et al., 1962) were produced by casting horizontally. This method was not widely used for water main pipes. Spun and pit cast grey cast iron are the two casting methods used to produce grey cast iron pipes for water mains.

In pit casting, chains of straight sand moulds were generated in a pit and the molten iron was poured into them. A metal flask lined with a thin coating of resin-bonded sand was employed as a mould. This method is called the mono-cast process. After the metal became cold enough, the pipes were taken out from the moulds (CSCE, 1916). In some cases, the pipes were subjected to heat treatment to lessen potential residual stresses, especially if metal moulds were employed to cast the pipes. The pit cast iron pipes were manufactured according to the ASA/AWWA A21.2/C 102-62 (1962) (Babbitt et al. 1962) and showed large differences in material homogeneity in addition to being heavier and more costly.

The other method called centrifugal pipe casting method was introduced in 1922 (CIPRA, 1967). Metal or sand moulds were used. In the first case, an amount of molten iron which has the suitable characteristics is poured into a rotating metal mould and provided with a socket core, so as to regularly spread the molten metal over the internal surface of the mould by the centrifugal force produced. A measured amount of molten iron was inserted into the spinning mould and the pipe was created by the centrifugal load. This load preserved the metal in place where it becomes cold

and solid. Once the metal hardens sufficiently to be handled, the mould is stopped and the pipe withdrawn. Decreasing the time frame between casting and spinning produce potentially thicker, smooth walls of uniform thickness (Babbitt et al., 1962).

1.3 Basic Mineralogy of Cast Iron

In general, cast iron can be defined as a large family of ferrous alloys. The chemical composition of cast iron is iron alloyed with carbon and silicon, which are present at a higher concentration than in steel. These lower the melting point of the alloy and increase its fluidity, allowing for easier molding into complex shapes such as pipes and fitting (Makar and Rajani, 2000).

Cast iron can be categorized according to the following standard types (Stefanescu, 1990):

1. Founded on fracture surface:
    - White iron: White iron shows a white crystalline fracture surface due to the fracture that occurs along the iron carbide plates.
    - Grey iron: Grey iron shows a grey crystalline fracture surface due to the fracture that occurs along the graphite plates (flakes).
2. Founded on micro structural features:
    - Graphite shape types: Lamellar (flake) graphite, spheroidal (nodular) graphite, compacted (vermicular) graphite, tempered graphite, and
    - Matrix type: Ferritic, pearlitic, austenitic, martensitic, bainitic.

3. Founded on commercial terminology

    - Common cast irons: in general study applications, unalloyed or low-alloy, being the ones employed for water main pipes, and
    - Special cast irons: In special applications, generally a high alloy.

Grey cast iron's composition shows a wide variety of carbon content as free carbon (graphite) in the form of flakes intermixed throughout the metal. The engineering properties of cast iron depend on these flakes (CIPRA, 1967). The different properties from those of steel are derived from the flakes. Cast iron is very brittle in nature; cracks can begin in the vicinity of the carbon flakes where stress occurs. In grey cast iron, fracture surfaces run preferentially from graphite flake to graphite flake. Therefore, their surfaces have the grey colour of graphite.

In addition to carbon, there are other chemical elements present in cast iron. These include silicon, manganese, sulphur and phosphorus. They are present in different amounts than they are in steel, which includes carbon(C) between zero and 2.0% and silicon (Si) between zero and 2.0%, whereas grey cast iron includes carbon (C) from 2.5% to 4.0% and silicon (Si) from 1.0% to 3.0% (Stefanescu, 1990). Silicon is responsible for the formation of detached graphite flakes. Silicon with a high amount of carbon is used to enhance the castability of the alloy.

Manganese sulphide also has an important role to play in controlling the effect of Sulphur on the alloy. On the other hand, sulphur will shape iron sulphide inclusions at the boundaries of the grains in the metal. Therefore, the cast iron becomes very brittle in behaviour and low in strength.

Phosphorus has a specific impact similar to that of sulphur if present in a large amount, as it shapes brittle iron phosphide (steadite) inclusions at the grain boundaries. Phosphorus works to increase the fluidity of the molten metal and enhances the abrasion and corrosion resistance. This is an advantage when manufacturing metal.

There are two fundamental materials (metal and graphite flakes) used to manufacture cast iron. The manufacturing method depends on the size and the shape of the graphite flakes as well as on the type of metal. During the manufacturing process, minimal cooling tends to produce large graphite flakes and ferrite (almost pure iron), modest cooling creates pearlite (alternating bands of ferrite and iron carbide in single grains) and smaller flakes, while fast cooling again generates ferrite but much thinner flakes of graphite (Makar and Rajani, 2000). As mentioned earlier, grey cast iron consists of graphite flakes and these influence mechanical properties.

1.4 Objectives

As discussed in the above section, cast iron pipe materials contain graphite flakes that vary significantly. Pit cast pipes contain much larger graphite flakes, which makes them susceptible to failure as they cause large cracks in the metal, and therefore reduce the mechanical strength. The mechanical properties of pipe materials are governed by the graphite flakes, their size and the metallic composition of the materials. As a result, the mechanical properties of cast iron pipe material vary significantly. However, limited information is currently available in the literature on the mechanical properties of the pipe materials as demonstrated by the lack of

published literature. In this research, the mechanical properties of a cast iron pipe's materials are determined. The specific objectives of the research are to:

- Conduct a physical examination of a cast iron pipe sample exhumed from a site after failure.
- Conduct laboratory testing to determine the mechanical properties of the pipe material.
- Conduct finite element modelling of the laboratory for interpretation of the test results.

The physical examination of the failed sample will improve understanding of the failure mechanism of cast iron pipe. Laboratory infestation will provide load-deformation behaviour that could be interpreted to determine material parameters based on simplified idealization. The developed material parameters will be evaluated and modified based on simulation of their observed behaviour using finite element modeling.

1.5 Organization of Thesis

The thesis is organized into five chapters. Chapter 1 illustrates the overall idea of the thesis. It includes the introduction of pipelines, manufacturing of cast iron pipes, basic mineralogy of cast iron, and objectives of this research. Chapter 2 presents a literature review on cast iron water mains, the failure of cast iron pipes and determination of mechanical properties. Chapter 3 describes the laboratory investigation used for this research and outlines the physical examination of a pipe sample, mechanical testing and interpretation of test results. Chapter 4 describes the

finite element modelling of the test performed. Chapter 5 includes conclusions from this research and recommendations suggested for future research.

Chapter 2: Literature review

2.1 Cast Iron Water Mains

Cast iron pipe is one of the most common water mains in North America, representing around 50% of the total length of built-up water main distribution pipes (Makar et al., 2001). Cast iron in water mains was used from the late 1800s until the late 1960s (Makar et al., 2001). Gray cast iron is a strong but brittle material (Najafi and Gokhale, 2005). There are two types of cast iron pipe, which are pit cast gray iron and centrifugal cast gray iron.

Being made of one of the oldest pipe materials, cast iron pipes in site are often deteriorated. As a result, a number of water main breaks occur across Canadian municipalities every year. There are several statistics on water main breaks in 21 Canadian cities for the years 1992 and 1993. The average break rate for cast iron pipe in 1992 was 56.16 breaks/100 miles/year and the average break rate for cast iron pipe in 1993 was 58.72 breaks/100 miles/year (Rajani and McDonald, 1993). Recently, Folkman (2012) performed a study on the failure rates of different cast iron pipe over a 12-month period. The failure rate for cast iron pipe was found to be 24.4 failures/100 miles/year (Folkman, 2012). Understanding the failure mechanism and prediction of pipes' structural condition is required for maintaining the integrity of water mains.

2.2 Failure of Cast Iron Pipes

There are many potential factors which might directly or indirectly contribute to pipe failure. A combination of corrosion and mechanical action is considered the major cause of pipe failure. Many types of failure such as circumferential and longitudinal breaking have been observed. Temporary repairs using a clamp are sometimes done. Figure 2-1 shows typical circumferential and longitudinal cracks along with temporary repairs.

Figure 2-1: Longitudinally cracked (84), circumferentially cracked (72), and temporarily repaired, clamped (71) Pipes (adapted from Seica, 2002)

Many of the pipes are expected to exhibit a broad range of mechanical properties in the water distribution network. The old pipes may have performed well over the years, but they may have a lower than anticipated strength. The age and loss of strength of the pipes may reduce the safety factors to potentially hazardous levels. Such pipes need to be identified as some of them may be subjected to higher-than-anticipated loads in certain locations and, as a result, the pipes may fail. Therefore, it is of the utmost importance to understand the mechanical properties of cast iron pipes in a particular distribution system. A better understanding of pipe failure mechanisms can lead to a realistic evaluation of the strength of the pipes in the system, and hence of their current level of safety.

Many studies have been conducted to explain and illustrate failure mechanisms of CI pipes. The failure methods and mechanisms normally noted in CI pipes have been abstracted in the literature. Makar et al. (2001) showed that large-diameter CI water pipes suffer from longitudinal fractures. The circumferential (hoop) stresses caused by internal liquid pressure and crushing forces drive longitudinal cracking. As such, longitudinal crackings are frequently related to internal pressure surges and/or unexpected crushing forces. Numerous longitudinal failures are noted to have nucleated from a region of significant wall thinning, usually due to advanced graphitization or pitting corrosion.

There are many parameters that determine the mechanical and metallurgical properties of CI water mains, such as age, location, and process (spun cast or pit cast) of manufacture. As an outcome of these wide differences, many investigations have concentrated on defining the metallurgical and mechanical properties of aging CI water mains (Makar and McDonald 2007; Seica and Packer 2004; Makar and Rajani 2000; Conlin and Baker 1991; Ma and Yamada 1994; Yamamoto et al., 1983). Different mechanical properties, such as ultimate tensile strength (UTS), the modulus of rupture (R), secant modulus of elasticity (E), Mode I fracture toughness (KQ or Kmax), and hardness, were measured in an attempt to explain the CI materials used in the water distribution networks presently in service. This database of material properties is very important for comparing with the limiting acceptance criteria and determining whether inadequate material properties may contribute to the failure of the pipe. There are many design specifications used to examine pipes (i.e., ASA/AWWA 1962a, b; USAS/AWWA 1967).

Gray cast iron is a non-homogenous, brittle material that behaves differently under tension and compression. The neutral axis in bending shifts towards the compression side because the gray cast iron presents nonlinear stress-strain characteristics（Shawki and Naga 1986).

In tension, most metals are more ductile than gray cast iron, because gray cast iron consists of a distribution of graphite flakes in an iron matrix. There is virtually no strength under tension in the graphite flakes. Stress concentrators and crack initiators that occur in the graphite flakes under loading lead to a reduction in mechanical properties. On the other hand, in regard to compression, stresses are transported by the graphite flakes. The most obvious macroscopic result is different strengths in tension and in compression, as well as different stress-strain behavior for the two loading conditions. Typically, the ultimate strength in compression may be two to four times the ultimate strength in the tension of the grey cast iron (Bauld 1986).

2.3 Research on Mechanical Properties

The mechanical characteristics of cast iron pipes are described in the ASA/AWWA (1962a, b) A21.6/C106-62 and ASA/AWWAA21.8/C108-62 specifications as a pair of tensile strength and modulus of rupture values (in ksi). Pit cast iron pipe is termed 11/31, and centrifugally cast iron pipe is referred to as 18/40. In USAS/AWWA (1967) ASA 21.1/H1-67, another higher grade pipe is referred to as 21/45. Table 2.1 shows the specific mechanical properties of cast iron pipes (tensile strengths, maximum values of the secant modulus) corresponding to the three grades of cast iron according to the specifications.

The behaviour of non-homogeneous cast iron material cannot be defined properly using the parameters stated in the specifications. Researchers have conducted

tensile and compressive tests of CI pipe specimens to accurately determine the material parameters. Fracture parameters for the material were also determined. Fatigue tests were performed on legacy CI water main materials (Mohebbi et al. 2010; Rajani and Kleiner 2010; Belmonte et al. 2009). The consequences of these investigations imply that the fatigue cracking in CI water mains is associated with subcritical crack growth. The stress intensity factors in pipes are unlikely to produce fatigue crack growth under reasonable operating conditions (loading) and initial defect sizes (corrosion pits and casting defects). Fatigue crack development would only be possible in situations with large defects or damage. However, the relatively large crack development in gray cast iron pipes results in quick crack propagation to a critical length and produces an unstable fracture. The presence of a corrosive environment within the crack provides an explanation for the gap in this observed behavior. Corrosion fatigue (CF) can potentially lead to subcritical crack development. Makar et al. (2005) indicated that several multistage failures depend on a mixture of a corrosive environment and cyclic loading. Jones (1996) also stated that brittle failure in CI pipes is due to the corrosion fatigue breaking point that is caused by the fluctuating tensile stresses in a corrosive environment.

Table 2.1: ASA/AWWA (1962a, b) A21.6/C106-62 and ASA/AWWA A21.8/C108-62 Specified Mechanical Properties of Cast Iron Pipes (adapted from Seica, 2002)

Grade of cast iron	Tensile strength (MPa/Ksi)	Modulus of rupture (MPa/Ksi)	Secant modulus at failure (MPa/Ksi)
11/31	75/11	215/31	$\leq 70000/10000$
18/40	125/18	275/40	$\leq 70000^{a}/10000$ or $\leq 83000^{b}/12000$
21/45	145/21	310/45	$\leq 70000^{a}/10000$ or $\leq 83000^{b}/12000$

a For pipes centrifugally cast in sand-lined molds.
b For pipes centrifugally cast in metal molds.

Some earlier research on the mechanical properties of cast iron pipe materials is briefly outlined below.

2.3.1 Kirby (1977)

Pit and spun methods were two methods used, by the Severn Trent Water Company in England to produce gray cast iron pipes and Kirby (1977) conducted tests with pipe specimens produced using these methods. These cast iron pipe specimens had both internal and external corrosion, since they had been installed between 1900 and 1958, and they were cut from water mains. Pipe diameters ranged from 75 to 150 mm (3 to 6 in). The tensile strength for uncorroded cast iron ranged from 150 to 170 MPa (22 to 25 ksi). The higher values for tensile strength were found in longitudinal specimens. These behaviors were described by Conlin and Baker (1991). The bending strength of cast iron is higher than its tension strength by about 25% due to the behavior of cast iron in tension and compression. Kirby (1977) investigated the tensile strength with corrosion pit depth and discovered a linear relationship between the two parameters that was not based on any structural or fracture mechanics concepts.

2.3.2 Yamamoto, Mizoguti, and Yoshimitsu (l983)

Yamamoto, et al. (l983) investigated specimens that were cut from cast iron pipes using static and fatigue tests. The pipe diameters ranged from 100 to 755 mm (4 to 30 in), and were installed from 1901 to 1958. The tensile strength of cast iron was measured by static tests to evaluate the impact of graphitization. The result of the tensile strength for uncorroded cast iron was approximately 140 MPa (21 ksi) and the approximate age of failure was (22 to 79 years). They reported a linear relationship between the tensile strength and the graphitization ratio, which are used to evaluate the structural condition of the water mains.

2.3.3 Caproco Corrosion Ltd. of Edmonton (1985)

Caproco Corrosion Ltd. of Edmonton (1985) conducted a number of tests. Specimens were removed from the spun cast iron water mains installed from 1957 to 1963 in Calgary, Alberta and the approximate age of failure (20 to 26 years). The tension test was performed to determine tensile strength, which was approximately 70 to 217 MPa (10 to 32 ksi).

2.3.4 The Philadelphia Water Department (1985)

Tensile strength was determined for cast iron water mains in the Philadelphia Water Department (1985). The dimensions of the pipes were not given. The age of the pipes was roughly between 20 and 130 years. The evaluation of the tensile strength of uncorroded cast iron was reported to depend on the age of the pipe specimens. The tensile strength of specimens from uncorroded pipe with an age of 35 years was 231 MPa (33.5 ksi).

2.3.5 Conlin and Baker (1991)

Conlin and Baker (1991) determined the tensile strength and fracture toughness of cast iron water mains. The tensile strength ranged from 137 to 212 MPa (20 to 31 ksi) and fracture toughness ranged from 10.5 to 15.6 MPa-$\sqrt{m}$ (9.6 to 14.2 ksi-$\sqrt{in}$).

2.3.6 Ma and Yamada (1994)

Cast iron specimens were cut from different locations along a 1,300 km (813 miles) long water distribution network in Nagoya, Japan. The tests were performed on cast iron specimens that were 89 years in-service. The tensile strength ranged from 40 to 320 MPa and the approximate age of failure was (21 to 32 years). The compressive strength and the fatigue behaviour were not studied.

2.3.7 Rajani et al (2001)

Rajani et al (2001) selected the pipes from four different locations within each distribution system in 16 water utilities across Canada and the United States to determine tensile strength and fracture toughness. The pipes were produced between the late 1880s and the early 1960s. DENT (double-edge notched tensile) samples were cut from pit gray cast iron pipes to obtain the fracture toughness values, which ranged from 5.7 to 13.7 MPa-$\sqrt{}$m. The tensile strength ranged from 33 to 267 MPa, and the secant elastic of modulus ranged from 38,000 to 168,000 MPa. The approximate ages of the pipes were 64 to 115 years. For spun gray cast iron pipes, the fracture toughness ranged from 10.3 to 15.4 MPa-$\sqrt{}$m, the tensile strength ranged from 135 to 305 MPa, and the secant elastic of modulus ranged from 43,000 to 159,000 MPa. The approximate ages of the spun cast pipes were 22 to 61 years. The large variability in data collected on tensile strength was explained by the fact that gray cast iron pipes were generally manufactured to meet or exceed minimum specified strength requirements, rather than falling within a range of specified strengths.

2.3.8 Seica and Packer (2002)

Seica and Packer (2002) performed mechanical tests on two types of cast iron pipe samples (pit & spun) that were received from different locations in Toronto, Ontario in Canada. The tensile strength from the tests ranged from 47 to 297 MPa and the secant elastic of modulus ranged from 23,000 to 150,000 MPa. The pipe samples were approximately 50 to 124 years of age at the time of the tests.

Table 2.2 shows a summary of the mechanical properties found by researchers and specified in standards:

Table 2.2: Comparison of Mechanical Properties of Cast Iron Pipes (Adapted from Seica1, 2002)

Type of Cast Iron	Reference	Specification/Feature	Tensile Strength [MPa]	Modulus of Rupture [MPa]	Secant Elastic Modulus [MPa]	Fracture Toughness [MPa √m]
Pit	ASA/AWWA A21.2/C 102-62	1939 to 1967	75	215	70,000	n/a
Pit	Rajani et. al. (2001)	Age; 66 -120 years	33 - 267	132 - 378	38.000-168,000	5.7 -13.7
Pit & Spun	Conlin and Baker (1991)	Out of service pipes	137 -212	n/a	n/a	10 .5 -15 .6
Pit & Spun	Seica1 and Packer (2002)	Age; 50-124 years	47-297	164 - 349	23,000-150,000	n/a
Spun	ASA/AWWA A21.6/C 106-62	1953-1982	125	275	83,000	n/a
Spun	ASA/AWWA A21.8/C 108-62	1953-1982	125	275	70,000	n/a
Spun	USAS/AWWA A21.1/H1 -67	1967-1982	145	310	93,000	n/a
Spun	Yamamoto et. al. (1983)	Age: 22 - 79 years	100 -150	20 - 250	n/a	n/a
Spun	Caproco Corrosion (1985)	Age; 22 - 28 years	70 -217	n/a	n/a	n/a
Spun	Ma and Yamada (1994)	Age; 21 - 32 years	40 - 320	120 - 320	n/a	n/a
Spun	Rajani et. al. (2001)	Age: 28 to 73 years	135 - 305	194 - 445	43,000-159,000	10.3 -15.4

Chapter 3: Laboratory Investigation

3.1 Introduction

The behaviour of buried pipes is governed by the mechanical properties of the pipe materials. Pipes buried in the ground are subjected to deterioration that may affect the mechanical properties of the material; however, the deterioration of pipe material properties has not been widely studied. The general approach used for analysis of the pipeline is to estimate the material parameters. Specific values of material parameters are used from the information available in the literature. However, researchers have indicated that material parameters for cast iron pipe materials vary widely and are nonlinear, (Shawki and Naga 1986). The stress-strain relation may also depend on the rate of loading. Loading rate dependent mechanical behaviour has not been investigated for cast iron pipe materials to date.

This chapter presents a laboratory testing program undertaken to determine the mechanical properties of cast iron pipe material that is approximately 40 years old. The pipe was exhumed from a site in the city of Mount Pearl in Newfoundland and Labrador after failure. The laboratory tests include physical examination of the deteriorated pipe, tensile tests of the specimens extracted from the pipe wall, a hardness test, and single-edge notch beam (SENB) tests. The effect of loading rate on the mechanical properties is also investigated.

3.2 Physical examination

Figure 3-1 shows the exhumed pipe sample; it is a cast iron pipe with nominal wall thickness of 10 mm. The pipe failed through longitudinal cracking. The

failure was due to extreme circumferential stresses resulting from high internal pressures.

The outside surface of the pipe wall was deteriorated due to corrosion. Figure 3-2 shows the deterioration of the pipe wall. However, no sign of significant deterioration was observed on the interior surface.

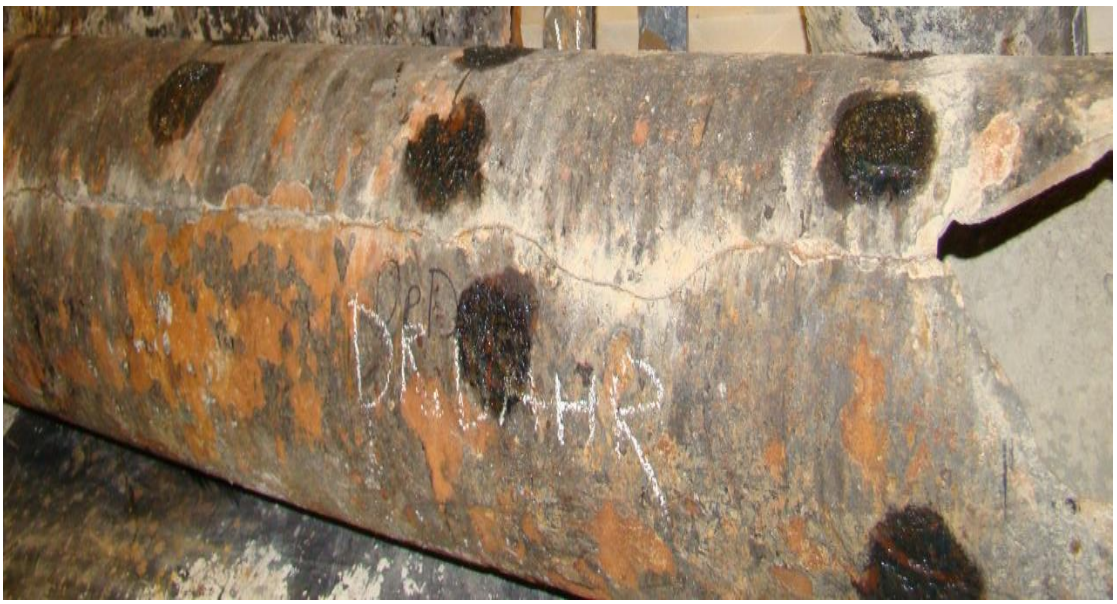

Figure 3-1: Pipe sample exhumed from the city of Mount Pearl

Figure 3-2: Deterioration on pipe wall

The failure mode of the pipe included longitudinal fracture and shear fracture, as shown in Figure 3-3. The longitudinal fracture was along the length of the pipe and oriented at 90° with the tangent to the pipe circumference. The shear/slant fractures were oriented approximately 45° with the longitudinal fracture on the outside surface of the pipe. The longitudinal fracture was measured to be approximately 97 cm long along the length of the pipe. A brown color was observed at around the middle of the crack. The brown-colored section was measured to be approximately 48 cm. The pipe wall thickness was reduced in the center of the brown-colored zone by approximately 30% to 50%, which was apparently caused by graphitization. A similar result was reported in a failed cast iron pipe in Cullin et al. (2015).

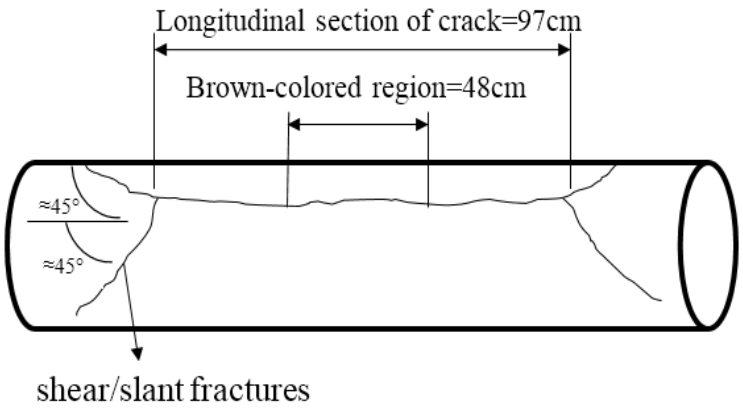

Figure 3-3: Schematic of the crack

To investigate the propagation of graphitization over the wall thickness, the pipe was cut with a water jet and then the cut surface was examined. Light surface corrosion and a minor external pitting corrosion were observed on the external surface of the pipe. Two clearly different colors were noticed on the fracture surfaces as shown in Figure 3-4 and Figure 3-5, respectively. The central part of the fracture

surfaces was darker brown-colored. The circumferential part of the fracture surfaces was lighter orange-colored. The presence of two different colours is due to corrosion, as also reported in Cullin et al. (2015). The colours varied depending on some smooth areas in the brown fracture surfaces, and the appearance was more homogeneous on the orange surfaces.

Figure 3-4: Brown-colored corrosion product on fracture surface

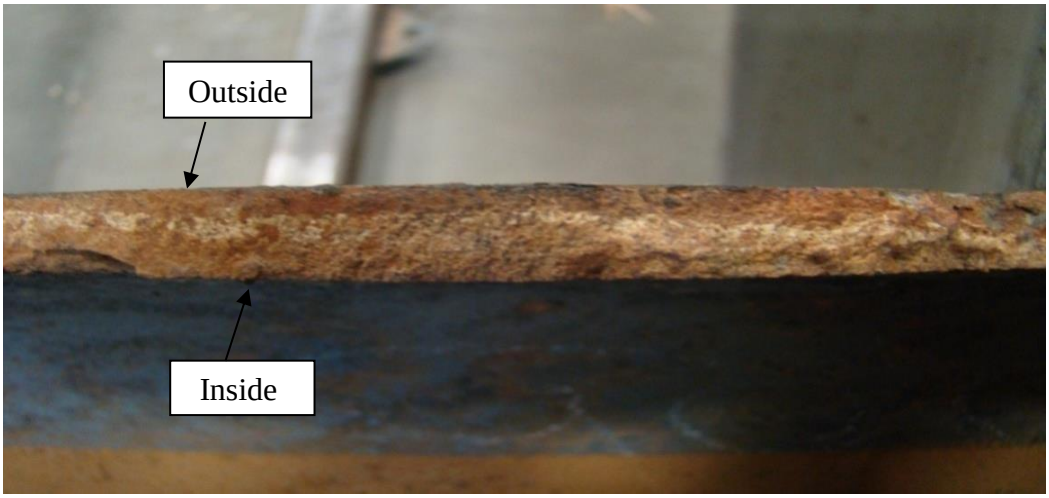

Figure 3-5: Orange-colored corrosion product on fracture surface

3.3 Material Defects

Localised defects were observed while preparing and milling mechanical test specimens. Figure 3-6 and Figure 3-7 show specimens with load defects. Hardness tests were conducted on the defective material and the intake pipe material. The results of hardness are discussed later in this chapter. Hardness was less prevalent on the defective material. The defect was on the inner surface of the pipe wall. The presence of the defect may be a result of manufacturing faults. This sort of defect may lead to subcritical crack growth.

Most of the defects were on the inner surface, which may be because the inner material solidifies last during manufacturing. In Figure 3-6, the defect was 4 cm long in the longitudinal direction of the pipe and permeated through almost half of the wall thickness. This defect may be subjected to water penetration through the pipe wall. The specimen shown in Figure 3-7 broke at the defect without any load, as shown in Figure 3-8.

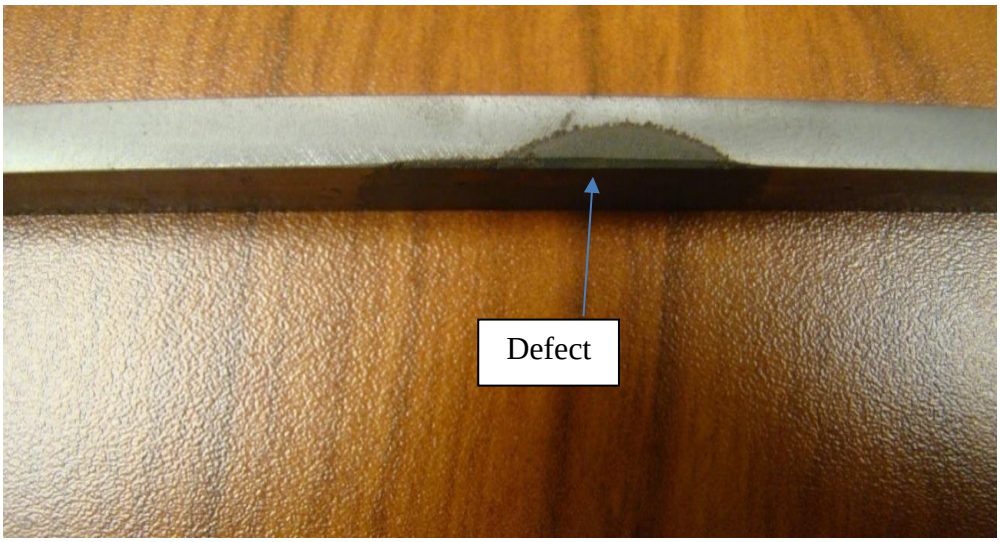

Figure 3-6: Defect observed during machining

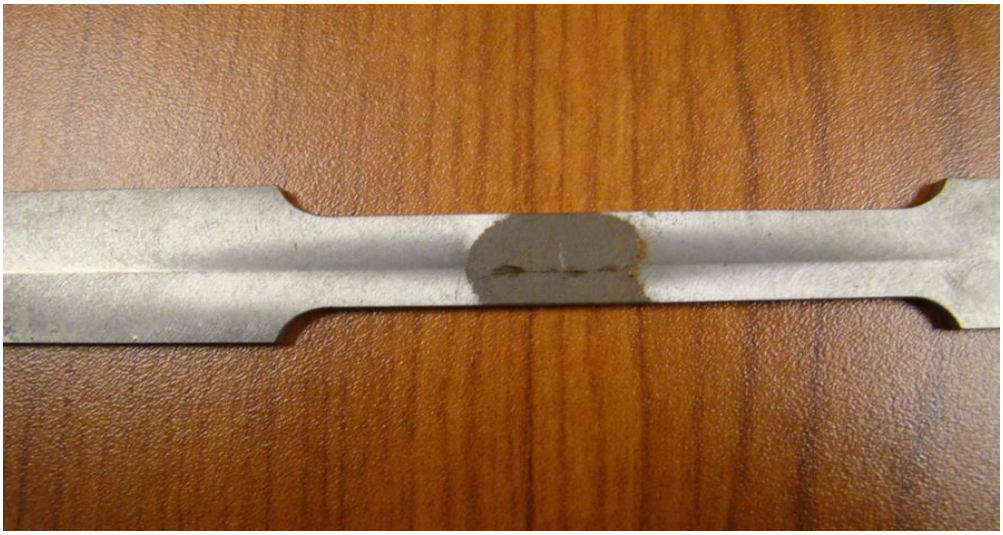

Figure 3-7: The defect observed at the middle of the tensile test specimen

Figure 3-8: The failure occurred at the defect

3.4 Mechanical Tests

A number of different tests are employed to determine the mechanical properties of cast iron. These include the determination of tensile strength, rupture modulus, ring bending strength, hardness, and fracture toughness. A specimen or coupon is cut from the pipe sample and is subjected to tensile load until failure in order to determine the tensile strength. Fracture toughness is a mechanical property that can be used to calculate the highest load that can be resisted by a grey cast iron pipe with known dimensions of corrosion pits. ASTM (2015), ASTM (2001) and AWWA (1975) standards are used for each of the mechanical tests to determine the specific material properties.

3.4.1 Tension Tests

The ASTM E8/E8M – 15 (2015) recommends different methods to determine the tensile strength of pipe material. The tension test sample is removed longitudinally or circumferentially from the midsection of the pipe wall. Flat or curved longitudinal tension test specimens can be used for a pipe with wall thickness less than 19 mm (3/4 in.).

There are two different dogbone-shaped specimens recommended for the tension tests. Round coupons are removed from the curved surfaces in the cross-section of the wall. Alternatively, flat coupons are removed as samples with standard cross-sections. The coupon has two shoulders and a gauge section in between. The shoulders have large cross-sections. The gauge section has a smaller cross-section so that deformation and failure can occur within this area. The main goals of using these specimens are to give a direct indication of the mechanical properties, as long as the

specimens have no manufacturing defects such as air inclusions. Corrosion products and any other material flaws visible on the flat coupons are removed.

There are advantages and disadvantages for each type of tension test specimens. The round coupons make it possible to have flawless specimens if the thickness of the pipe is limited and manufacturing defects exist (not sufficient material). Flat coupons are considered suitable when flawless specimens can be machined.

All the tensile tests in this research were performed on flat gray cast iron specimens that had been cut from different locations of the pipe wall. The specimens length were parallel to the length of the pipe. Figure 3-9 shows the flat coupons machined. The specimens did not contain any corrosion-affected areas or manufacturing defects (air inclusions, foreign body inclusions, etc.) particularly within the gauge length. A sample with a defect within the gauge length was also obtained, as discussed earlier in Figure 3-7.

Figure 3-9: Flat grey cast iron specimens

Tests were performed using an INSTRON (5585H) machine. Displacement controlled tests were carried out with a displacement rate of 0.5 mm/min, 1 mm/min, 10 mm/min and 20 mm/min, respectively. A typical tensile test set-up is shown in Figure 3-10.

Figure 3-10: Test setup for tensile test

Eleven specimens were processed from the cast iron pipe sample. Before the test, the dimensions for all specimens were measured within the gauge length.

An extensometer was used to measure the axial deformation and strain. Strain gauges were also used to verify the strains measured by the extensometer in a few tests. Biaxial strain gauges were used to facilitate calculation of Poisson's ratio. The extensometer and strain gauges set-up are shown in Figure 3-11.

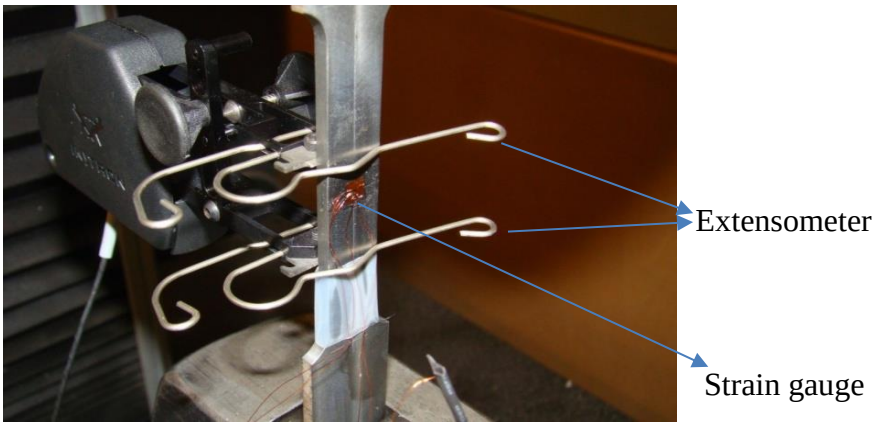

Figure 3-11: Set-up of extensometer and strain gauge

Load-deformation and load-strain response were obtained using data acquisition systems. Engineering stress and engineering strain were then calculated from the data.

Although the objective of this research is not to study the effect of cyclic loading, four tension test specimens were tested under repeated loadings to develop a preliminary understanding of the loading-unloading response of the material. Two of the tension specimens were loaded at a displacement rate of 0.5 mm/min and 1 mm/min. Two others tension specimens were loaded at a displacement rate of 10 mm/min and 20 mm/min, respectively.

Since the stress-strain relations were non-linear, two modules of elasticity were calculated from the stress–strain relationships obtained from the experiments. The initial tangent modulus (Young's modulus) is calculated as the initial slope of the linear of portion from the stress vs. strain curve. The secant modulus is defined as the slope of a straight line from the origin to the point of failure of the stress-strain curve.

3.4.2 Hardness testing

ASTM standards E18 – 15 (2015) recommend a method to determine the Rockwell hardness of pipe material. Hardness is the property of a material that enables it to resist plastic deformations caused by indentation. However, the term hardness may also indicate resistance to bending, scratching, abrasion or cutting.

The method used to obtain a hardness value is to compute the depth or area of an indentation left by an indenter of a specific shape, which is created by a specific force applied for a specific time. There are three principal standard test methods for

expressing the relationship between hardness and the size of the impression: Brinell, Vickers, and Rockwell hardness numbers.

In this research, Rockwell hardness was used as illustrated in the ASTM E18 – 15 (2015).

For Rockwell hardness measurements, the load presses the indenter down against the specimen with a minor load of 10 kg for 3 seconds. The feedback from the force sensor is used to control the load. Then, the load is increased for 3 seconds to the major loads of 60, 100, or 150 kg depending on the scale used.

Rockwell hardness values are designated as a composition of a hardness number and a scale symbol representing the indenter and the minor and major loads. The hardness number is expressed by the symbol HR and the scale designation.

Most applications are covered by the Rockwell A, B, and C scales for testing steel, brass, and other metals. Additionally, each steel ball indenter has a diamond indenter that is different in diameter (1/16, 1/8, 1/4 and 1/2 in).

For soft materials, such as copper alloys, cast iron, soft steel, and aluminum alloys, a 1/16" diameter steel ball is used with a 100-kilogram load and the hardness is read on the "B" scale.

The hardness tests were conducted using a Wilson hardness testing machine. During the tests, a 1/16" hardened steel ball indenter applied a minor load of 10 kg for 3 seconds, and a major load of 100 kg for 3 seconds. The hardness was read on the "B" scale because the material was cast iron. The load was applied at the limits specified by ASTM E18 – 15 (2015). Measurements were taken at different locations

of the flat specimen (three measurements in each shoulder and three in the small area). A typical test setup for a hardness test is shown in Figure 3-12.

Figure 3-12: Test setup for Hardness Test

3.4.3 Single Edge Notch Beam (SENB) Tests

A Single-Edge Notch Beam (SENB) Test is performed according to the standards of ASTM E 1820-01 (2001). According to this standard, a linear load-displacement is specified for a valid measurement of fracture toughness. An initial pre-crack is encouraged by fatigue to ensure a sharp pre-crack. However, fatigue pre-crack was not applied for the tests conducted here, since the fracture toughness for cast-iron pipe material was estimated to be low based on a preliminary Charpy test result. Thus, the sample might break during the standard pre-cracking stage. The standard process for measuring fracture toughness is to use a single-edge notched bend (SENB) specimen (ASTM E 1820-01).

In this research, single-edge notch beam (SENB) tests are performed. The specimens, which were removed from the pipe as rectangular cross-sections, had a span that was parallel to the length of the pipe. The experimental specimen was produced from the complete wall thickness of the pipe. Corrosion spots noticed during sample preparation were removed through machining. A pre-cracking notch (V-notch) was nominally prepared on the specimens to the specified dimensions, as reported in Mohebbi et al. (2010). Then, tests were conducted for different depths of the V-notch. A typical SENB specimen is shown in Figure 3-13.

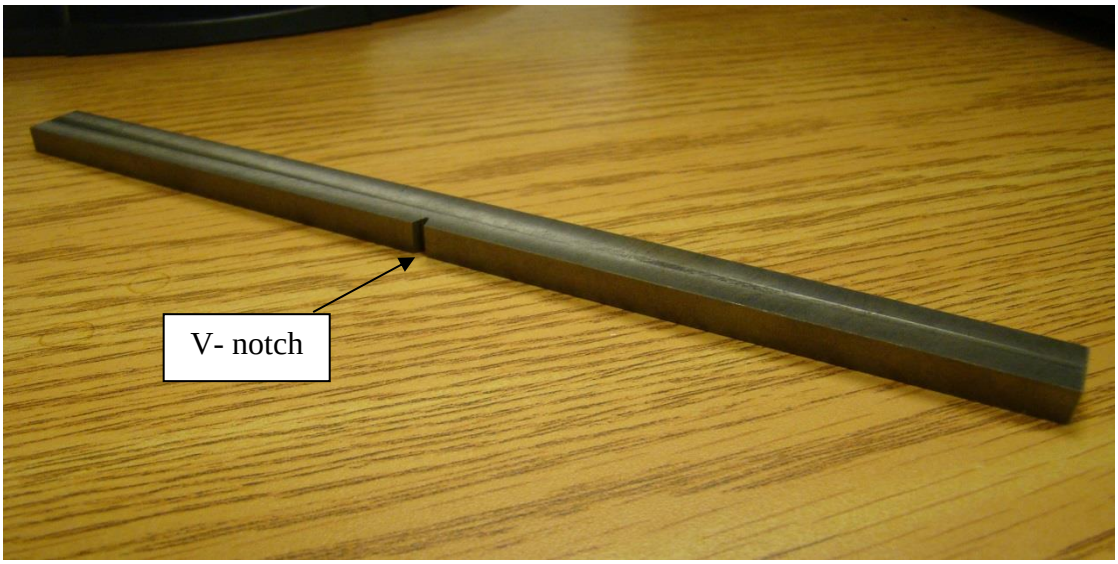

Figure 3-13: SENB Test Specimen

The samples were tested using the testing set-up shown in Figure 3-14. A three-point loading method was used according to the requirements of ASTM E 1820-01 (2001). The fracture toughness K_C was then estimated from the ultimate force P, using Eq.3.1, (Mohebbi et al. (2010)).

$$K_C = \frac{PS}{BW^{3/2}} f(a/w) \tag{3.1}$$

In Eq (3.1), S is the clear span of the specimen, B is the thickness, W is the depth, and $f(a/W)$ is given by (Mohebbi et al. 2010):

$$f(a/W) = \frac{3(a/W)^{1/2}}{2(1+2a/W)(1-a/W)^{3/2}} * (1.99 - (a/W)(1-a/W)(2.15 - 3.93a/W + 2.7a^2/W^2)) \quad (3.2)$$

Where a is the crack length

The SENB test specimen dimensions were 14 mm thick, 7 mm wide, and 84 mm long. Notches were made with depths of 3.2 mm for two specimens, 4.7 mm for four specimens, 6 mm for two specimens and 7.5 mm for two specimens. A total of ten specimens were tested.

The SENB specimen was put on two supports (simple support) and was subjected to a load at one point at the middle of the span until failure.

In a few tests, two strain gauges were attached at two different locations of the specimen to measure strain distribution. One of the strain gauges was attached on a surface near the notch and the other was attached on the opposite side of the specimen at the middle of the cross-section (at the expected neutral axis) as shown in Figure 3-15. A linear voltage displacement transducer (LVDT) was mounted to measure displacement, as shown in Figure 3-14. A data acquisition system was used to read the strains and the displacement.

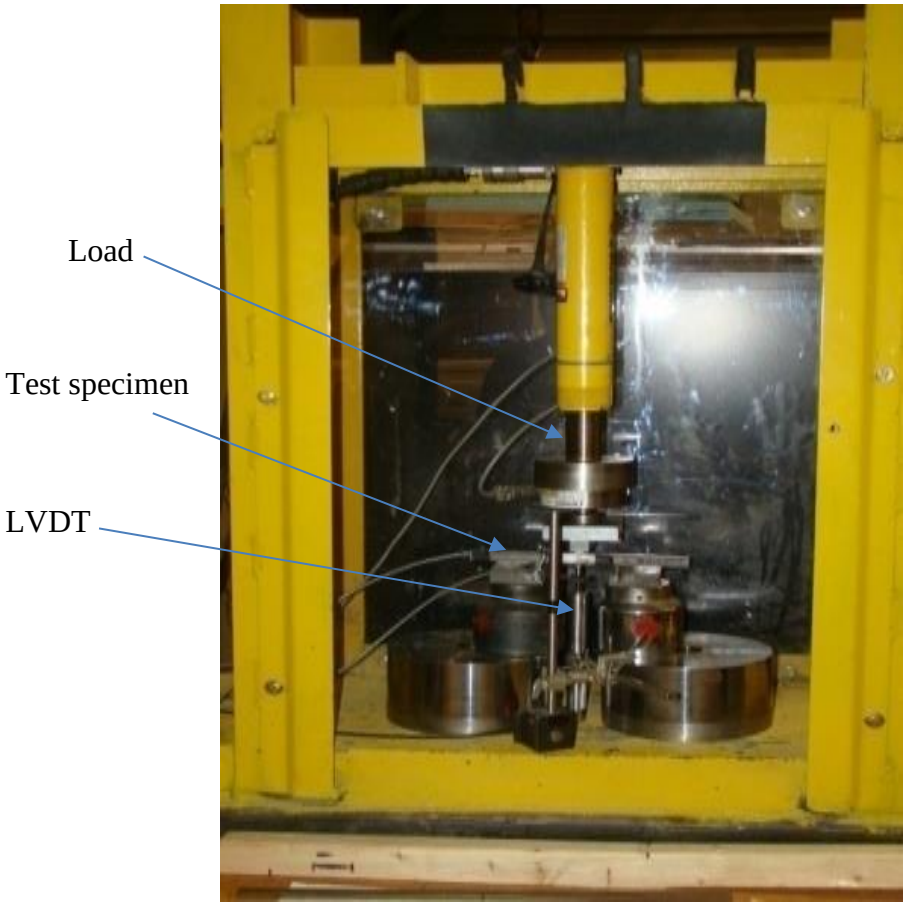

Figure 3-14: Test setup for SENB Test

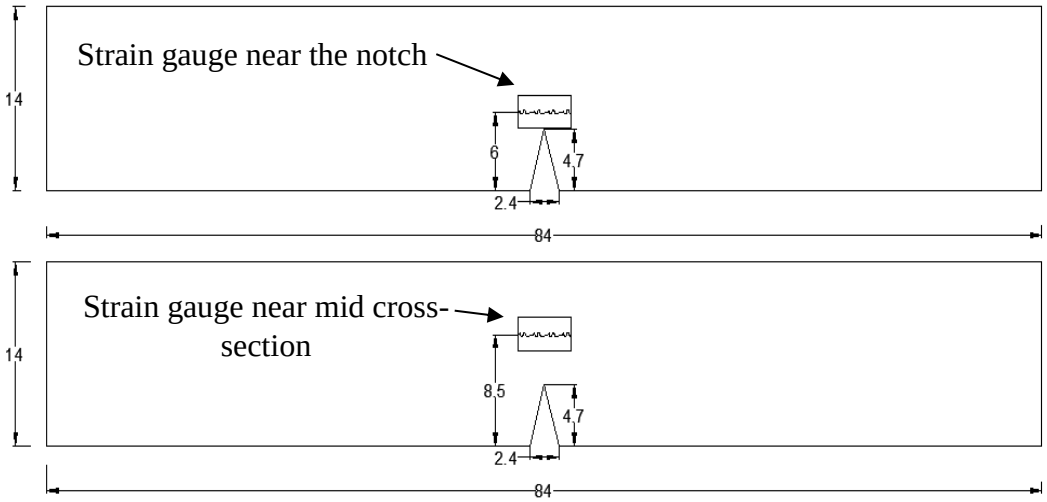

(All dimension are in mm)

Figure 3-15: Setup of two strain gagues for SENB test specimen

3.5 Results of Tension Tests

Tension tests were performed on specimens extracted from the pipe at different displacement rates. The detailed program of the Tension tests is summarized in Table 3-1. Tests 1 to 5 are the preliminary tests conducted to evaluate the performance of the test facility including the extensometer, is used for measuring deformations and strains. The preliminary tests reveal that the leg of the extensometer may slip during the test, affecting the deformation and strain measurements. The extensometer legs slipped during Test 2 and Test 4. Deformations and strains from these tests are therefore not available. For the subsequent tests, the surfaces of the test specimen are made rough using sand paper to ensure proper grip of the extensometer.

Table 3.1: A Summary of Tensile Test Program

Test ID	Date of test	Width within gauge length	Thickness within gauge length	Rate of loading	Strain gauge used or not
1	September 2, 2015	12.6 mm	3.11 mm	10 mm/min	No
2 Slipped	September 14, 2015	12.7 mm	3.23mm	1 mm/min	No
3	September 15, 2015	12.64 mm	3.28 mm	1 mm/min	No
4 Slipped	September 25, 2015	12.71 mm	3.18 mm	20 mm/min	No
5	October 9, 2015	12.6 mm	3.11 mm	20 mm/min	Yes
6	November 9,2015	12.6 mm	3.11 mm	20mm/min	Yes
7	November 23,2015	12.6 mm	3.11 mm	10 mm/min	Yes
8	May 11, 2016	12.74 mm	3.22 mm	0.5 mm/min	No
9	May 11, 2016	12.74 mm	3.21 mm	1 mm/min	No
10	May 11, 2016	12.64 mm	3.1 mm	10 mm/min	No
11	May 11, 2016	12.62 mm	3.22 mm	20mm/min	No

Figure 3-16 shows the stress-strain relations obtained from Test 1, 3 and 5. Test 1, 3, and 5 were conducted at strain rate of 20 mm/min, 10 mm/min and 1 mm/min. The stress-strain responses are very similar to the strain rate of 20 mm/min and 10 mm/min for these cases. However, as discussed later, different stress-strain response are concentered for loading rates of 20 mm/min and 10 mm/min. The same response observed for the loading rates of 20 mm/min and 10 mm/min in Figure 3-16 is attributed to the variable of the material. The stress-strain response is softer for the loading rate of 1 mm/min. The stress-strain response thus appears to depend on the loading rate. In Figure 3-16, the stress-strain response is initially linear up to a stress of 50 to 80 MPa. Beyond that point, the stress-strain response is nonlinear. From the stress-strain relation, Young's modulus of elasticity, yield strength and ultimate strength are determined, which are presented later is this chapter.

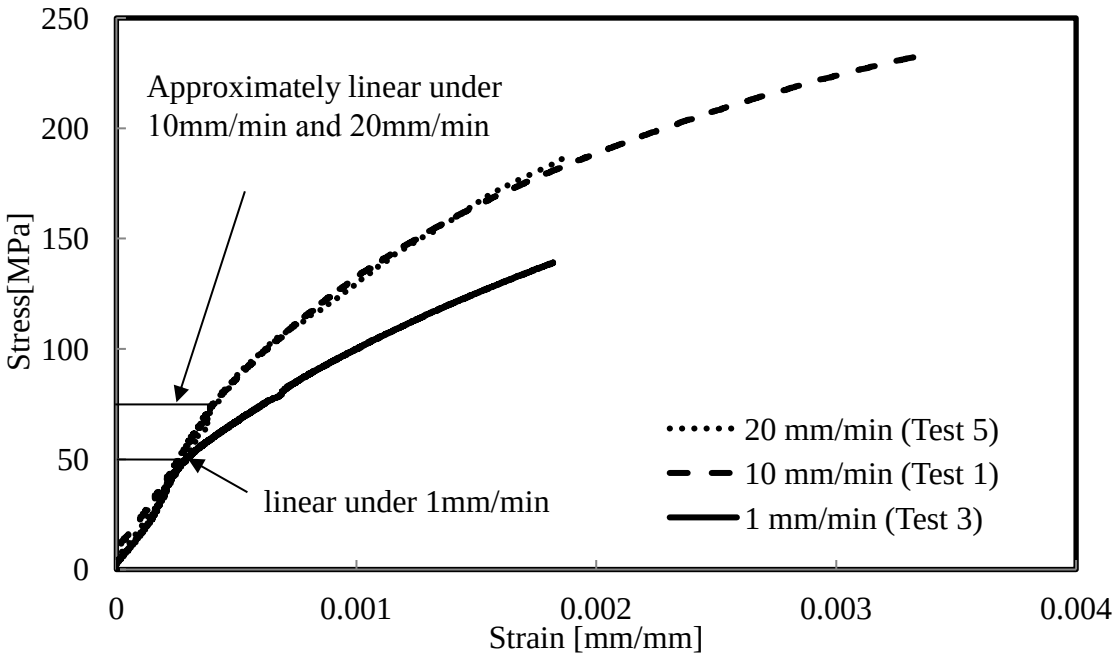

Figure 3-16: Stress-strain plot Tests 1,3 and 5

In Tests 6 and 7, biaxial strain gauges were attached to the specimen near the centre to measure strains. The strains measured using the strain gauges and the extensometer were compared. However, the extensometer slipped during Test 6 and measurements from the extensometer are not available. Figure 3-17 shows a comparison of stress-strain responses obtained using strain gauges and the extensometer from Test 7. Strains measured using the extensometer and strain gauges appear to be close to each other in the figure.

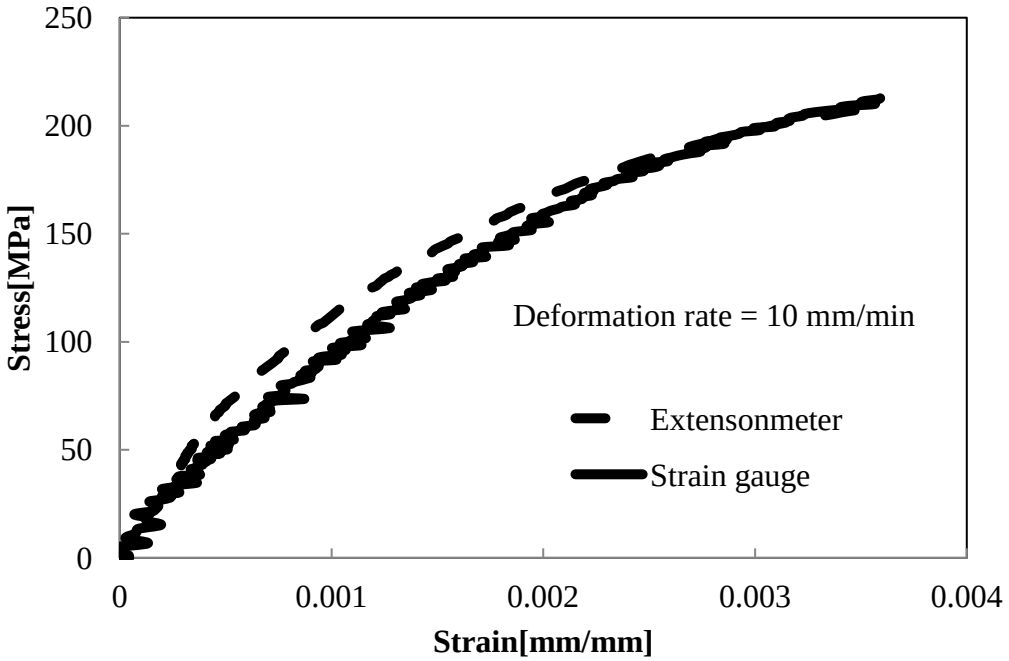

Figure 3-17: Comparison of strain measured using extensometer and strain gauge

Tests 8 to 11 were used to investigate the strain rate effects on the stress-strain behaviour. Tests were conducted at a loading rate of 0.5 mm/min, 1 mm/min, 10 mm/min, and 20 mm/min, respectively. The tests revealed the material strengths of cast iron as 175 MPa, 163 MPa, 179 MPa, and 195 MPa from tests 8, 9, 10, 11, respectively.

Figure 3-18 plots the stress-strain relations obtained using different strain rates from a separate set of tests (test 8 to 11) conducted for this purpose. The stress-strain relations are nonlinear, as is expected for cast iron pipe material, and are affected by the rate of loading (strain rate). The initial slope of the stress-strain response is higher for a higher loading rate. As a result, ultimate tensile strength is also higher. The stress–strain behavior is linear within an initial region. Beyond that region, the stress-strain relationship changes to nonlinear. The initial tangent modulus is calculated from the slope of the linear portion of the stress-strain relations. Ultimate strength σ_u and the failure strain ε_u are computed at the point of the failure. The secant modulus E_s at the point of failure is also determined.

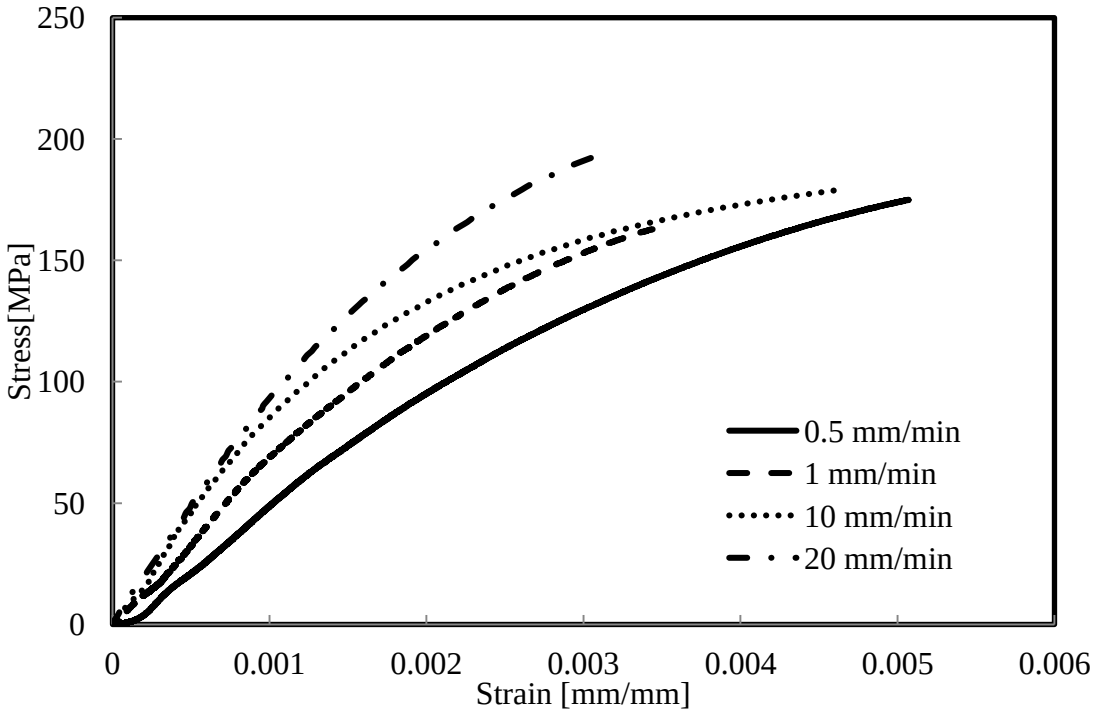

Figure 3-18: Stress-strain plot from Tests 8,9,10 and 11

Figure 3-19 explains the determination of the initial tangent modulus and yield strength. Figure 3-20 shows the determination secant modulus. Mechanical parameter thus determined are discussed in the following sections.

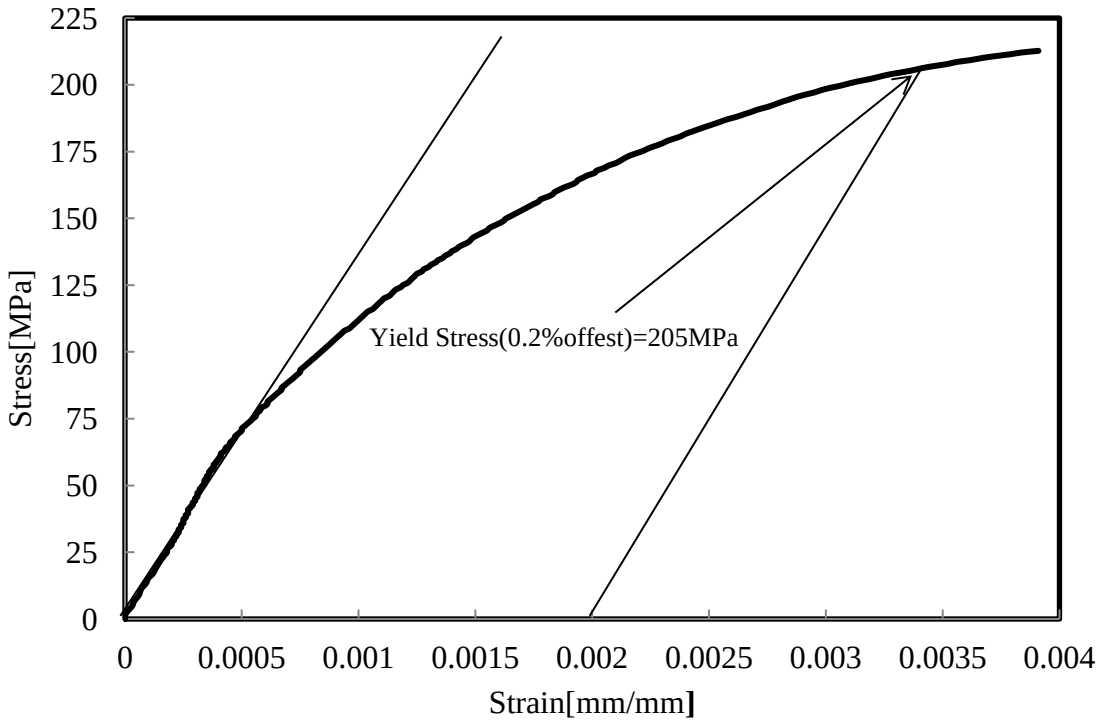

Figure 3-19: Determination of yield strength

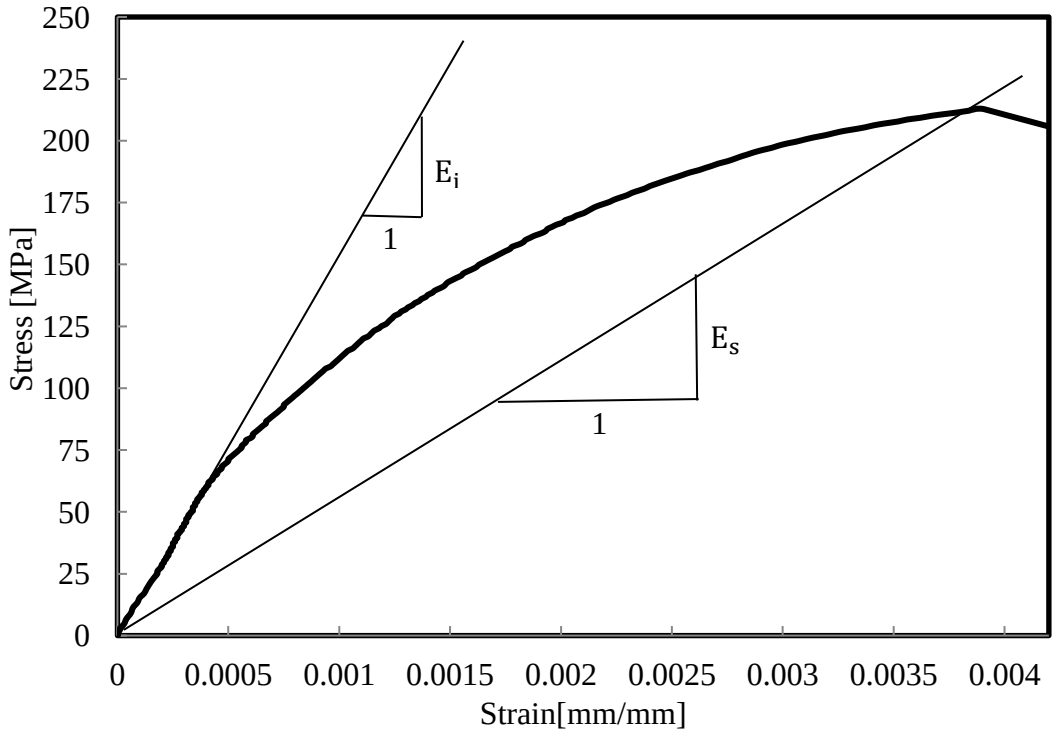

Figure 3-20: Determination of initial modulus and second modulus

3.5.1 Mechanical Properties

Table 3.2 summaries the mechanical parameters obtained from the tensile tests. The material parameters appear to vary for the samples obtained from different locations of the same pipe, indicating that the material properties vary from point to point.

In general, the moduli of elasticity and ultimate strengths are higher for a higher loading rate. For a loading rate of 20 mm/min, the initial modulus varies from 98 GPa to 185 GPa and the ultimate strength varies from 184 MPa to 195 MPa. For the loading rate of 10 mm/min, the initial modulus and the ultimate strength ranges from 91 GPa to 186 GPa and from 179 MPa to 234 MPa, respectively. Thus, the material parameters obtained from the loading rate of 20 mm/min and 10 mm/min are not significantly different.

For a loading rate of 1 mm/min, the initial modulus varies from 69 GPa to 169 GPa and the ultimate strength varies from 139 MPa to 163 MPa. At a loading rate of 0.5 mm/min, the initial modulus and the ultimate strength were 69 GPa and 163 MPa, respectively.

It appears that although the initial elastic modulus is affected by the rate of loading (strain rate), the ultimate strength of the material does not significantly vary with the loading rate. Figure 3-21 shows the variation of ultimate strength obtained from different tests. Based on the test results, the ultimate strength varies from around 150 MPa to around 200 MPa. The average and the standard deviation for ultimate strength were calculated to be 185 MPa and 27, respectively. The failure strains at the ultimate strength vary from 0.002 to 0.005.

Table 3.2: Mechanical properties obtained from tensile tests.

Specimen NU#	Test ID	Rate mm/min	E_i GPa	σ_u MPa	ε_u	E_s GPa
1	1	10	186	234	0.0034	69
2	3	1	169	139	0.0018	76
3	5	20	185	186	0.0019	100
4	6	20	163	184	0.0021	86
5	7	10	150	213	0.0039	54
6	8	0.5	49	175	0.0051	34
7	9	1	69	163	0.0034	47
8	10	10	91	179	0.0046	39
9	11	20	98	195	0.0032	61

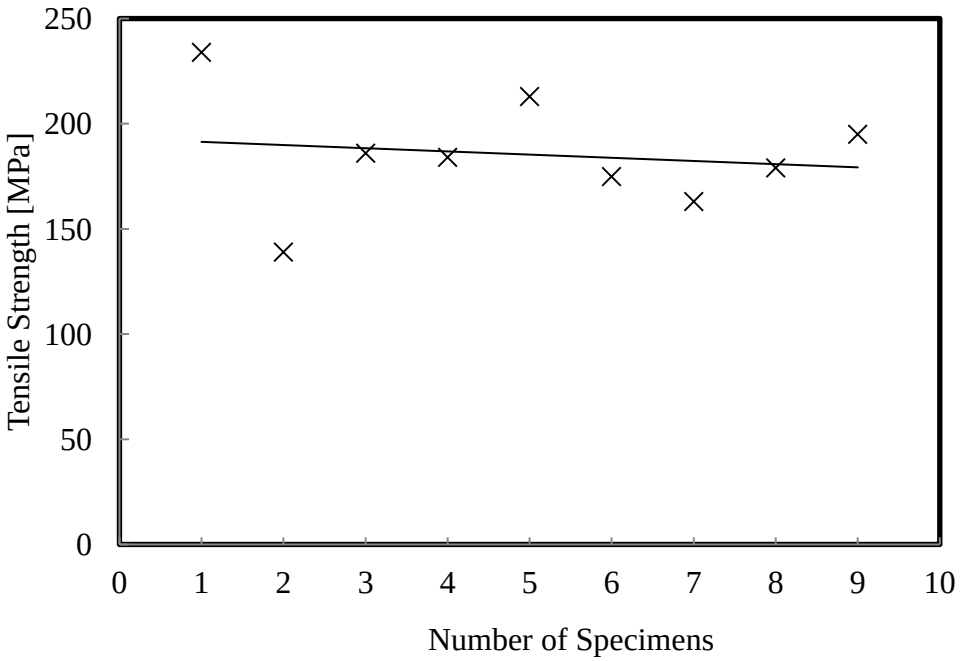

Figure 3-21: Distribution of the Tensile Strength for the Tested flat Tension Specimens

3.5.2 Poisson's ratio

To facilitate the calculation of Poisson's ratio, longitudinal and lateral strains were measured using a biaxial strain gauge in two of the tests. The stress-strain relations are plotted in Figure 3-22 and Figure 3-23. In these figures, the strain in the

longitudinal direction is non-linear with stress. However, the lateral strain varies linearly with the stress. This implies that the stress-strain relation is non-linear for extension and predominantly linear for compression.

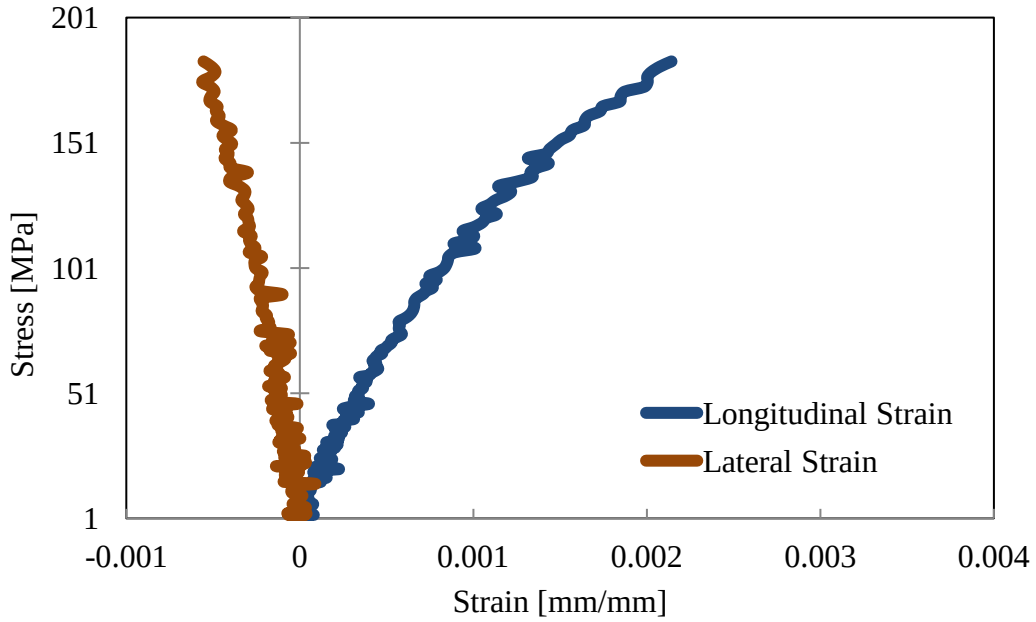

Figure 3-22: Stress-strain plot from Test 6 (Deformation rate 10 mm/min)

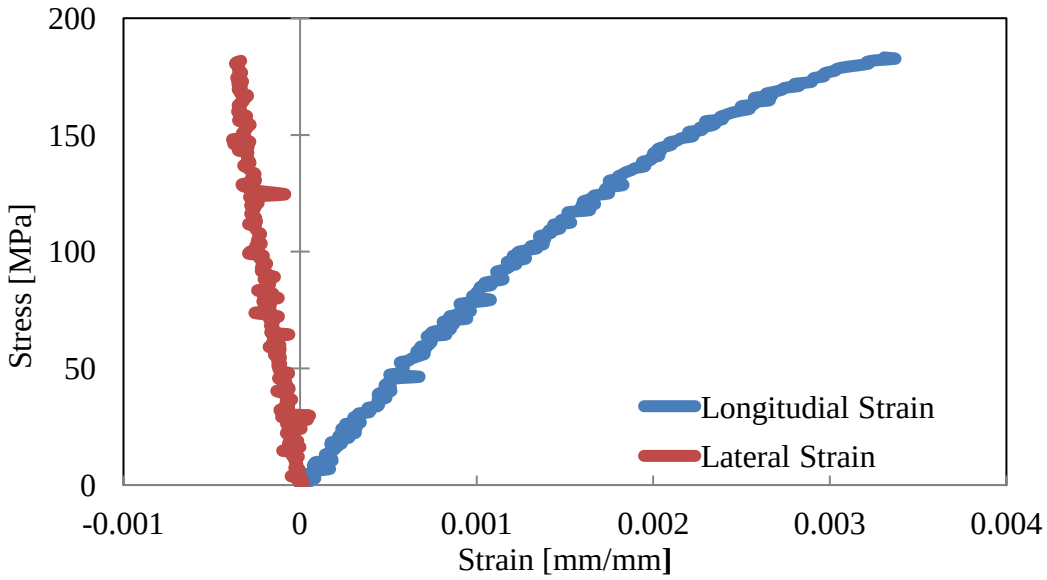

Figure 3-23: Stress-strain plot from Test 7 (Deformation rate 20 mm/min)

The ratio of the lateral to longitudinal strain is used to calculate the Poisson's ratio of the material. Figure 3-22 and 3-23 show the Poisson's ratio when

displacement controlled tests were carried out with a displacement rate of 20 mm/min and 10 mm/min, respectively. In Figure 3-24, the Poisson's ratio ranged from 0.32 to 0.29 and the average and the standard deviation for the Poisson's ratio was calculated to be 0.32 and 0.02, respectively. In Figure 3-25, the Poisson's ratio ranged from 0.34 to 0.22 and the average and the standard deviation for the Poisson's ratio were calculated to be 0.25 and 0.03, respectively.

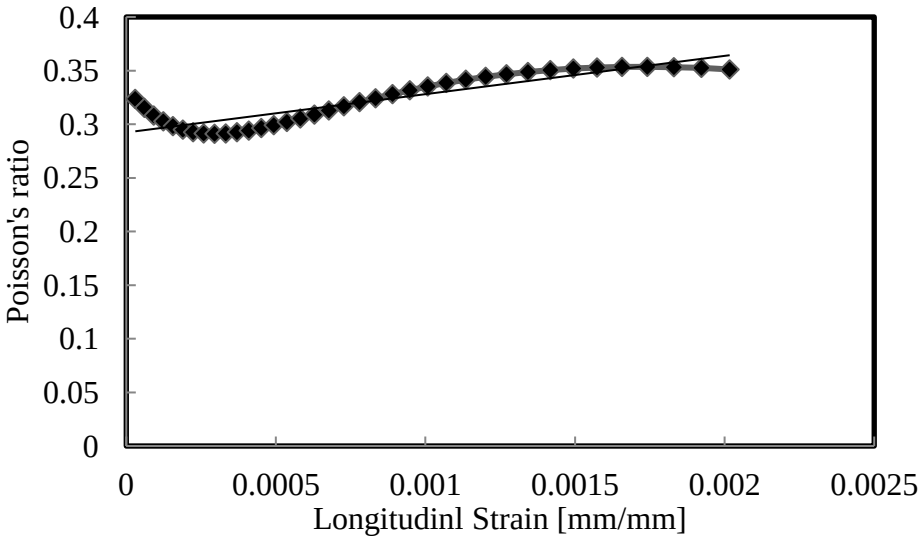

Figure 3-24: Poisson ratios from Test 6

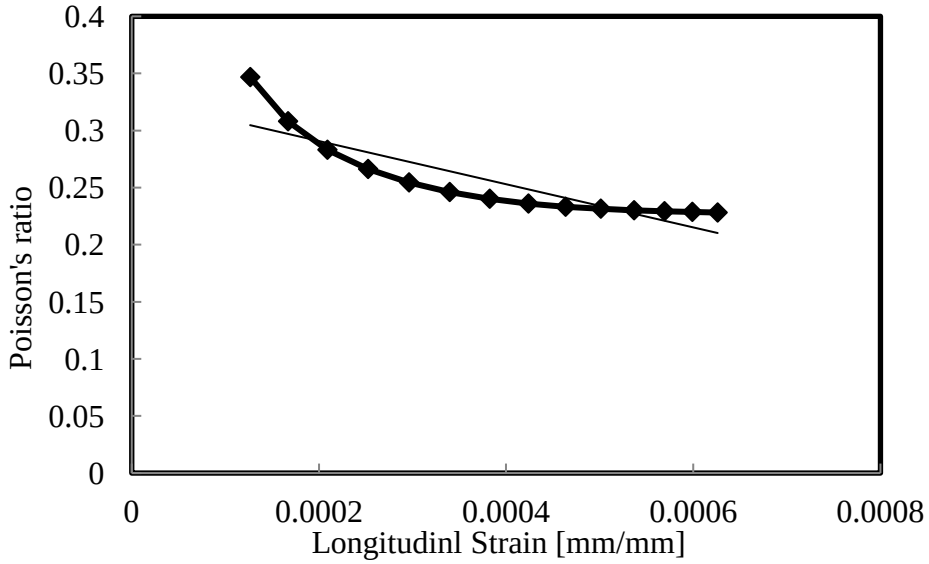

Figure 3-25: Poisson ratios from Test 7

3.5.4 Unloading-Reloading Behaviour

Stress-strain relationships for repeated loadings are illustrated in Figure 3-26 to Figure 3-29. The detailed program of the tension tests with unloading-reloading is summarized in Table 3-3. While the data is not sufficient to understand the unloading-reloading behaviour well, it appears that within the tension zone, the unloading-reloading line is parallel to the initial straight line. However, within the compression zone, the response is stiffer.

Table 3.3: Summarized Tension Test Program with unloading-reloading

Test ID	Date of test	Width within gauge length	Thickness within gauge length	Rate of loading
1UR	April 22, 2016	12.7 mm	3.18 mm	0.5 mm/min
2UR	April 22, 2016	12.7 mm	3.18mm	1 mm/min
3UR	April 22, 2016	12.7 mm	3.18 mm	10 mm/min
4UR	April 22, 2016	12.7 mm	3.18 mm	20 mm/min

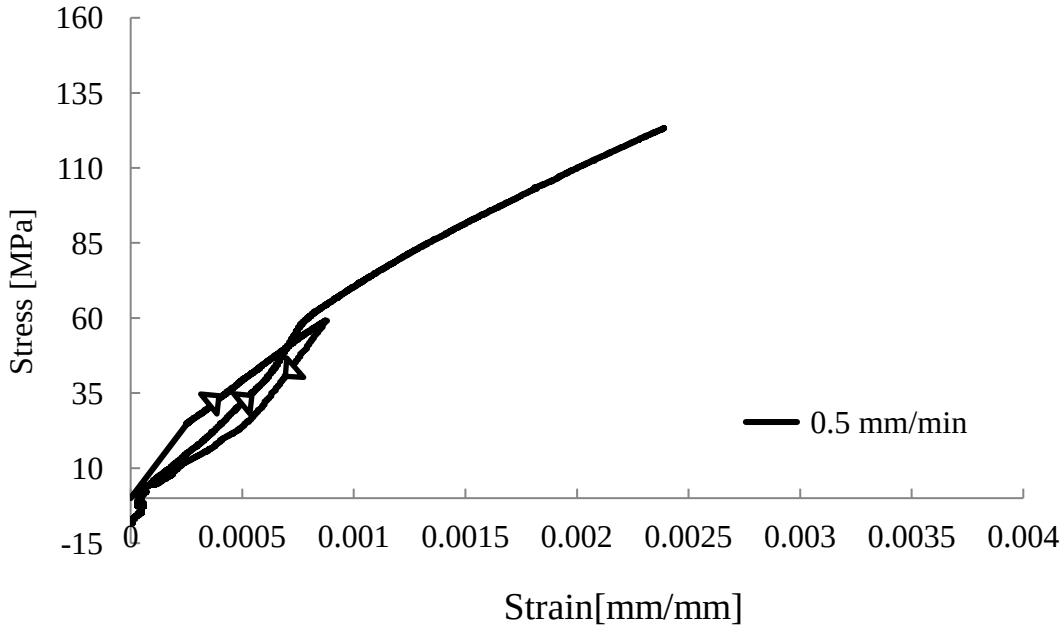

Figure 3-26: Stress-strain data for unloading-reloading Test 1UR

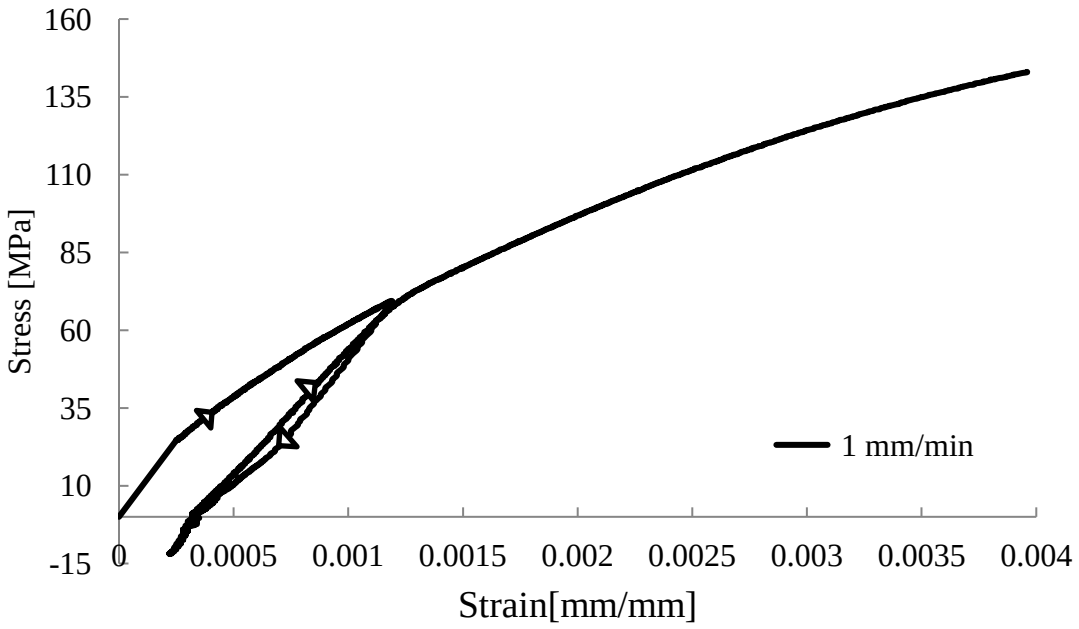

Figure 3-27: Stress-strain data for unloading-reloading Test 2UR

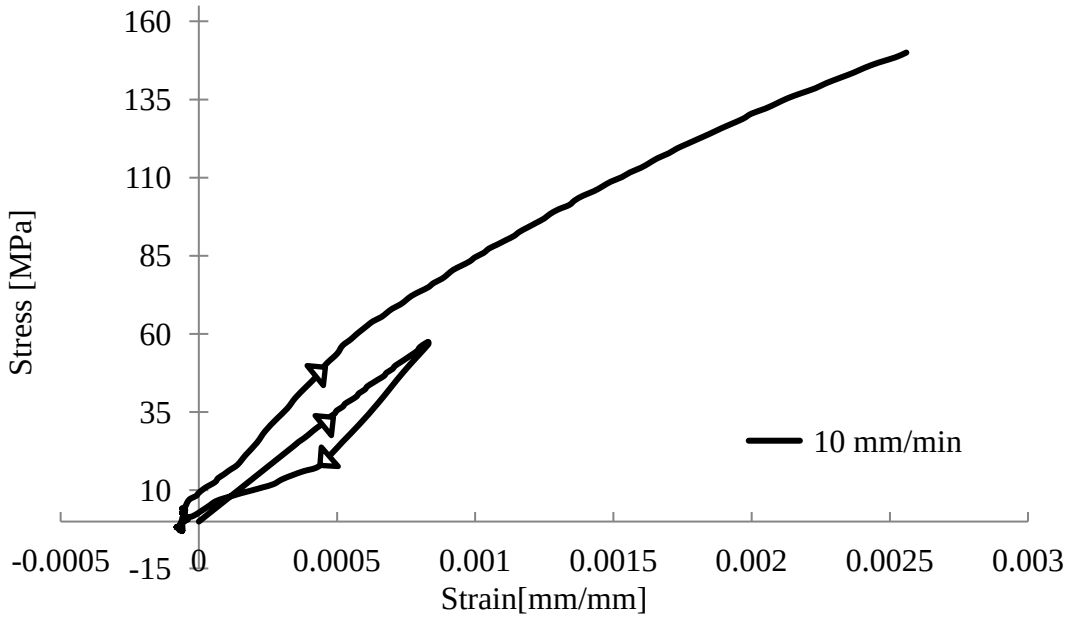

Figure 3-28: Stress-strain data for unloading-reloading Test 3UR

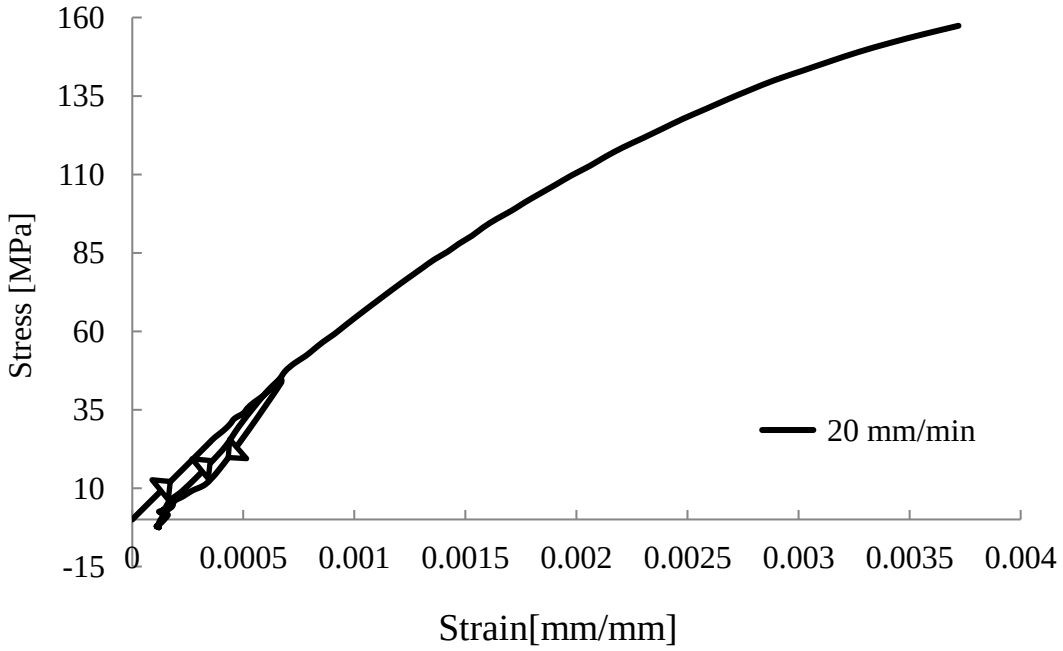

Figure 3-29: Stress-strain data for unloading-reloading Test 4UR

3.6 Results of Hardness Tests

The results of hardness test are shown in Figure 3-30. The hardness values obtained from the tests are very similar and range from 80 to 88. These values are within the range specified in AWWA (1975).

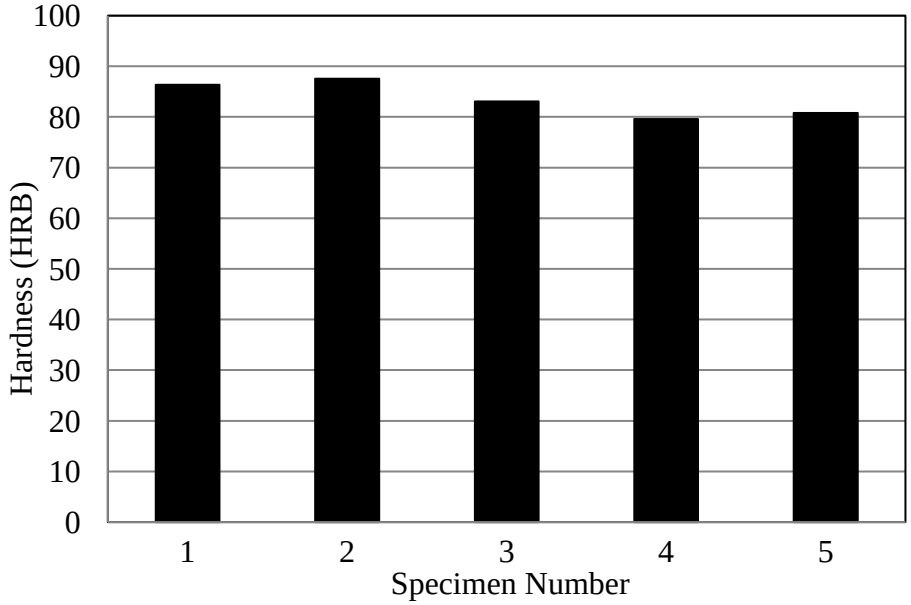

Figure 3-30: The values Rockwell Hardness

3.7 Results of SENB Tests

SENB tests were conducted on specimens extracted from different locations of the pipe. Tests were conducted in accordance with ASTM E 1820-01(2001). The width to depth ratio (W/B) of the test specimen were in the range $1 < W/B < 2$. The minimum thickness of the specimens (B) is recommended to be $B > 2.5(K_C / \sigma_{ys})^2$, where K_C is fracture toughness and σ_{ys} is yield stress, as reported in Mohebbi et al. (2010). For the tests conducted $2.5(K_C / \sigma_{ys})^2$ is calculated to be 0.0004 to 0.0012, which are smaller than the width (B) of the beam.

Specimens with notches of 3.2 mm, 4.7 mm, 6 mm and 7.5 mm were tested. Figures 3-31 to 3-34 show typical load-displacement data during the single-edge notch beam (SENB) tests for ten specimens with different notch depths that were investigated. SENB tests with different notch depths are conducted to identify the effect of depth (i.e. crack length) on the fracture toughness of the cast iron pipe material. It should be noted that Eq (3-1) for the fracture toughness evaluation was developed for ductile material. The application of Eq (3-1) for brittle cast iron material is evaluated through the evaluation of K_C for different notch depths. Figures 3-31, 3-32, 3-33 and 3-34 plot the load-displacement response for a notch depth of 3.2 mm, 4.7 mm, 6 mm and 7.5 mm, respectively. In general, an increase in the notch depth corresponds to an increase in displacement and a decrease in failure load.

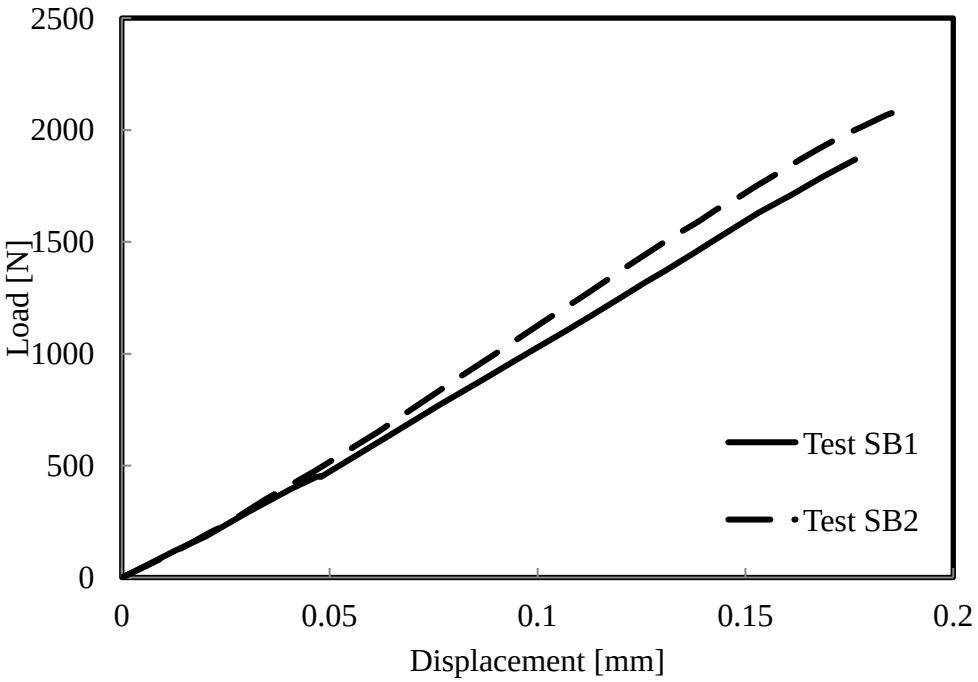

Figure 3- 31: Load-Displacement for a Notch Depth of 3.2mm

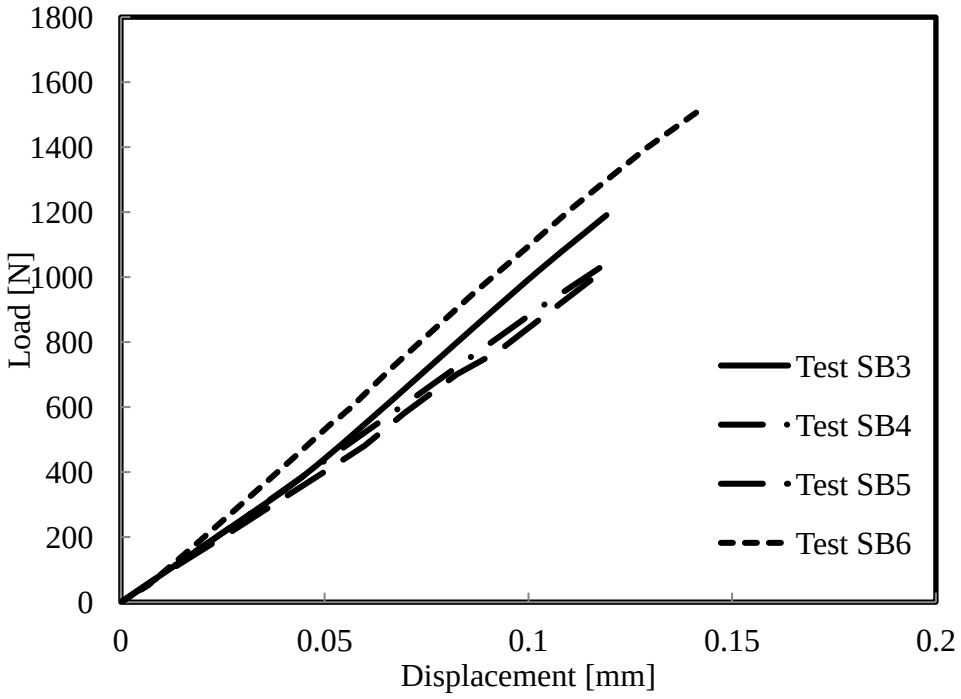

Figure 3-32: Load-Displacement for a Notch Depth of 4.7mm

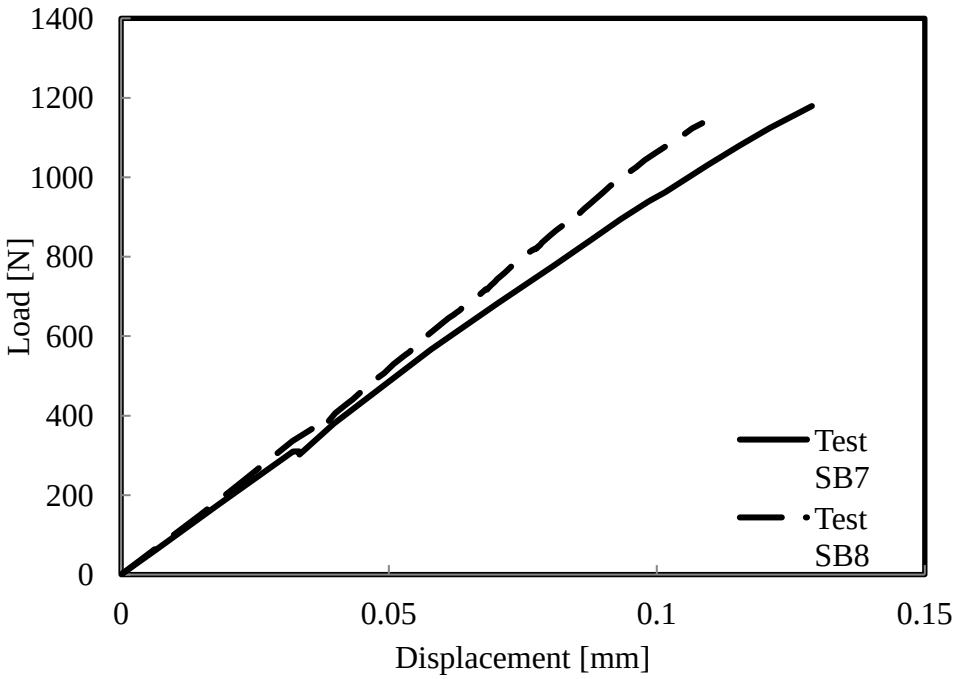

Figure 3- 33: Load-Displacement for a Notch Depth of 6mm

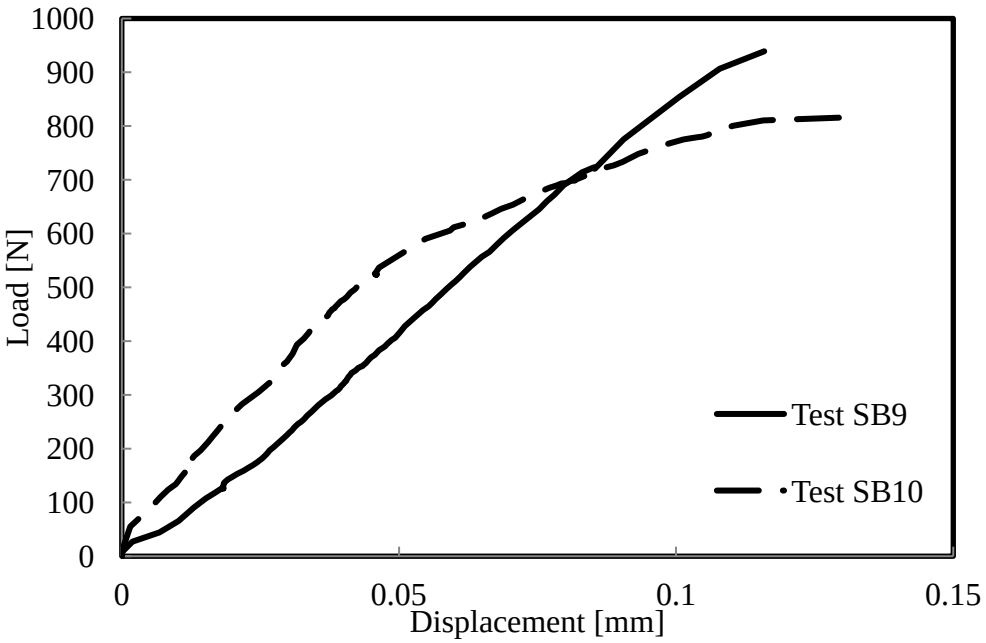

Figure 3-34: Load-Displacement for a Notch Depth of 7.5mm

The load-displacement curves presented in Figures 3-31 to 3-34 show a semi-linearity. A non-linear load-deflection relation in a single-edge notched bend (SENB) is expected for cast iron pipe material in bending due to different material behavior in tension and compression. Figure 3-35 shows the stress distribution on a cross-section of a cast iron element subjected to pure bending (Shawki and Naga, 1986). Non-linear behaviour of cast iron under tensile stresses can be observed in Figure 3-35. A small amount of non-linearity is also exhibited in the compression zone. The dotted line in the figure shows the stress distribution within the section for a typical material having similar linear material properties in tension and compression.

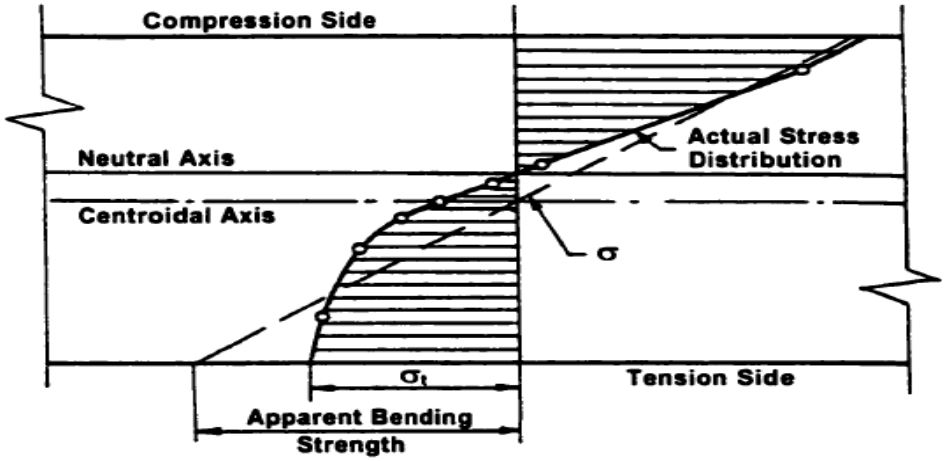

Figure 3-35: Comparison between Actual and Ideal Linear (Apparent) Stress Distributions in Flexure(Adapted from Shawki and Naga, 1986)

From the load-deflection response (Figures 3-31 to 3-34), the load and deflection at failure are obtained. The failure loads and the deflection are used to calculate the ultimate flexural strength σ_u of the material and the modulus of elastically. The ultimate flexural strength is calculated using the linear beam theory.

$$\sigma_{ys} = \frac{M}{I} \quad y \tag{3.3}$$

The equation can be expressed as follows:

$$M = \frac{P*L}{4} \tag{3.4}$$

$$I = \frac{b*w^3}{12} \tag{3.5}$$

Where:

σ_{ys} = Cross-sectional tensile or compressive stress [MPa];

M = Applied bending moment [N-mm];

y = Distance from the centroidal axis to the point where the stress is calculated [mm];

I = Moment of inertia of the cross-section [mm^4];

P = Total applied force [N];

L = Length of specimen (distance between supports) [mm] ;

B = thickness of the specimen [mm];

W = width of the specimen [mm];

The Young's modulus can be obtained by using Equation (3.6) for the elastic vertical displacement at the centre of a beam applied to a three-point bending load:

$$\Delta center = \frac{PL^3}{48E_iI} \tag{3.6}$$

Where:

$\Delta center$ = Elastic vertical displacement at the centre of a beam subjected to three-point bending [mm];

I = Moment of inertia of the cross-section [mm^4];

P = Total applied force [N];

L = Length of specimen (distance between supports) [mm];

The slope of a tangent line for the load-displacement curve at the point of origin is the initial tangent modulus of the material that can be computed by the following equation:

$$E_i = \frac{\left(\frac{P}{\Delta center}\right) L^3}{48I} \quad (3.7)$$

Where, $\left(\frac{P}{\Delta center}\right)$= the slope of the initial tangent line to the load-displacement curve [N/mm].

Table 3.4: Mechanical Properties of Cast Iron from single-edge notched bend (SENB) tests

Test #	a mm crack length	Failure Force P N	Δcenter	K_C N/mm$^{3/2}$	σ_u Stress MPa	Initial Tangent Modulus [GPa]
SB1	3.2	1869	0.17	4.75	374	178
SB2	3.2	2106	0.19	5.35	421	187
SB3	4.7	1191	0.12	6.31	329	263
SB4	4.7	1068	0.12	5.66	295	230
SB5	4.7	1020	0.12	5.4	282	227
SB6	4.7	1523	0.14	8.07	421	280
SB7	6	1179	0.13	12.82	580	378
SB8	6	1136	0.11	12.36	559	433
SB9	7.5	939	0.12	13.65	862	625
SB10	7.5	816	0.13	11.86	749	484

Fracture toughness is also calculated using Eq (3-1), as is discussed earlier. Table 3.4 summarizes the material parameters obtained from tests. The flexural strength of the material is found to vary from 282 MPa to 749 MPa, the Young's modulus varies from 178 MPa to 484 MPa and the fracture toughness varies from 4.75 $N/mm^{3/2}$ to 13.65 $N/mm^{3/2}$. The fracture toughness K_C evaluated using Eg (3-1) appears to depend on the depth of the notch. K_C is higher for greater depth (or higher crack length) for the cast iron pipe material. The Young's moduli in Table 3.4 are much higher than the moduli of elasticity obtained from the tensile tests (Table 3.2). The type of loading appears to have an effect on the material parameters determined. The type of stress developed within the specimen are different in the tensile test and SENB test. In the tensile test, the specimen is subjected to uniform tension. However, in the SENB test, the portion of the cross-section above the neutral axis is subjected to compression while the portion of the section below the neutral axis is subjected to tension. As discussed earlier, material behavior under tension and under compression are different for cast iron pipe material.

To investigate the mechanism of deformation further, the distribution of strain with the distance from the neutral axis is investigated for the SENB test. Strain measurements at two points along the line of the load are available from one of the tests. The strain gauge is placed near the notch, and at around the middle of the depth at the section. The location of the strain gauges is shown in Figure 3-15.

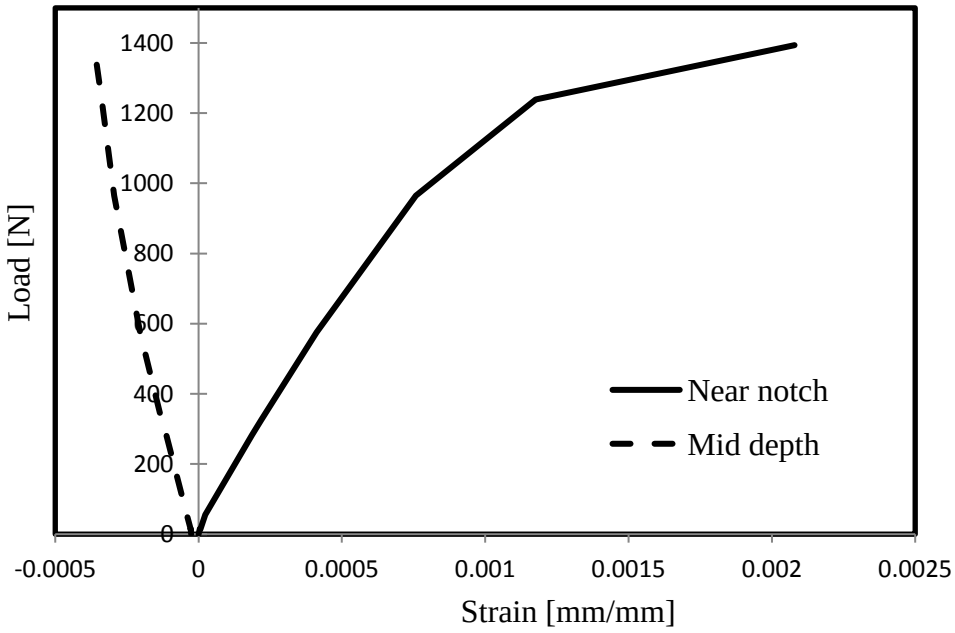

Figure 3-36: shows the strain at deferent locations of the specimen

Figure 3-36 plots the load-strain relations obtained from the strain measurements. The figure reveals that the strain near the mid-depth of the beam, which is under compression, increases linearly with the load. The increase of strain near the notch is non-linear with the load. This again indicates that the stress-strain behavior in tension is non-linear for cast iron. The stress-strain relation in compression can be idealized as linear. The strain measurement near the notch can be affected by the geometry of the notch as well. This is discussed further in Chapter 4.

It also should be noted that the strain is non-zero at the mid-depth of the section; thus, the neutral axis is not located at the mid-depth. This is attributed to the different stress-strain response of the material and the presence of the notch.

Chapter 4: Finite Element Modelling

4.1 Introduction

In Chapter 3, a laboratory investigation carried out to determine the mechanical properties of cast iron pipe material is described. Specimens under tension and in bending were investigated. The failure mechanism observed during the tests were different from the mechanism expected for ductile materials. Tests are analyzed in this chapter using the finite element method to evaluate the determined material parameters in simulating under the loading conditions during the experiments.

The finite element method is an effective tool used to model complex mechanical behaviours. Different modelling techniques are used to model the non-linear stress-strain behaviour, complex geometry of the problem and the failure criteria. Although the stress-strain response is non-linear, a common approach in modelling cast iron material for finite element analysis is to use linear stress-strain relation, a constant yield stress and a constant ultimate stress. Wang et al., (2000) employed material parameters based on the typical values in finite element modelling of cast iron camshafts. The material parameters were: ultimate tensile strength of 249 MPa, Young's modulus of 170,000 MPa, Poisson's ratio of 0.29, and yield strength of 202 MPa.

Josefson et al., (1995) employed different yield stresses in tension and compression for cast iron material. The yield stress that results from compression is generally greater than the tension due to the presence of micro-cracking in the pearlitic matrix of the graphite flakes (Josefson et al., 1995).

Hjelm (1994) and Josefson et al. (1995) used the yield criteria in modelling non-linear kinematic hardening using the program ABAQUS. Figure 4-1 shows the yield criteria suggested, which are based on the von Mises-type yield condition. In this figure, the yield stresses in the tension and in the compression of cast iron are 100 MPa and 300 MPa, respectively. Figure 4-1 shows the yield loci under biaxial loading. The first failure criterion (solid line) is a "shifted" von Mises condition that was found to provide an overestimation of the compression-compression zone (Hjelm, 1994). To overcome this, a modified "shifted" von Mises criterion (dashed line) was used. The model, however, underestimated the true behavior of cast iron in the tension-tension zone (Hjelm, 1994). The best fit to the experimental results was found to be obtained in the tension-tension zone, if a Mohr-Coulomb (or Tresca with different yield strengths in tension and compression) yield surface (dotted line) had been used (Hjelm, 1994).

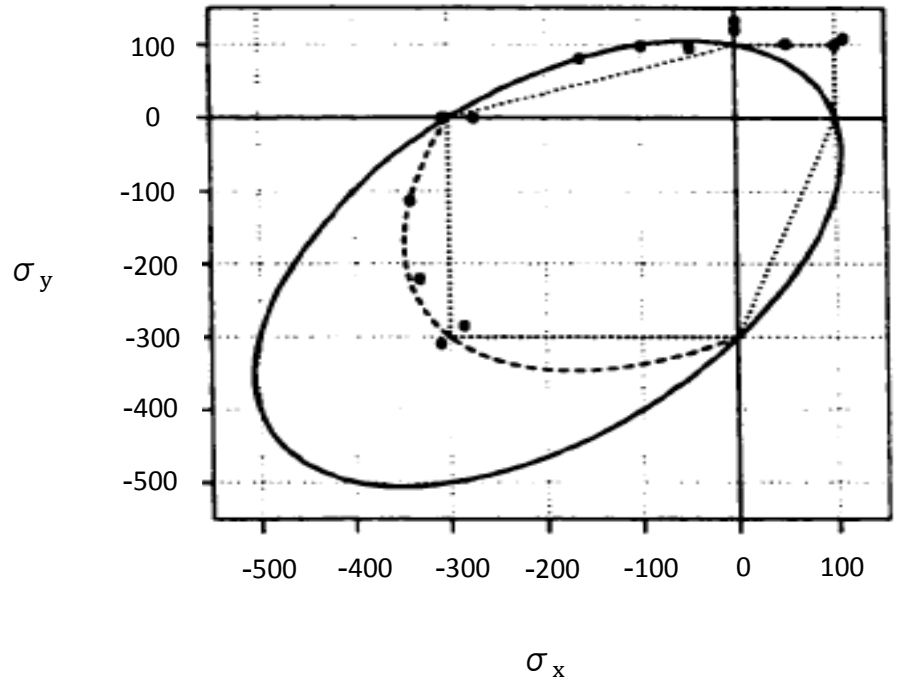

Figure 4-1: Modified von Mises and Mohr-Coulomb Yield Criteria for Grey Cast Iron (adapted from Hjelm, 1994)

Hjelm (1994) indicated that it is difficult to determine a yield stress point on the tensile stress-strain relationship using the experimental test results for cast iron. The yield point cannot be determined since the curve does not show the threshold**.** In using the 0.2% offset method, two problems are encountered: (i) even at very low stress, the stress-strain relationship continues changing the slope and an initial tangent slope cannot be determined. As a result, the yield stress is dependent on an acceptable evaluation of the initial slope of the stress-strain curve; and (ii) in a tension test, the test specimen may fail before a 0.2% offset-based yield point is reached.

Hjelm also (1994) suggested fitting the stress and strain data from experimental to a polynomial function and computing the point of maximum curvature of this function. This suggestion can be used to determine the onset of plastic deformation. The method was good for curves of compressive stresses, but was not always successful for tension stresses.

Cast iron is a material that exhibits brittle failure, which is correlated to the tensile strength. Seica (2002) used data acquired from uniaxial tensile tests to model a non-linear elastic material property curve. However, as cast iron presents a certain amount of plasticity and because of the energy-conservative characteristic of the constitutive material behavior, unloading was not analyzed.

In this research, the stress-strain behaviours of cast iron pipe materials are investigated and simplified material parameters are determined in Chapter 3. This chapter presents finite element analysis of the tests conducted to evaluate the performance of the determined parameters in simulating the test conditions. The failure mechanism observed during the tests are also investigated.

4.2 Finite Element Software

The finite element software was chosen based on a few considerations. Firstly, a software that is well-accepted in the industry is considered. Secondly, the capability of the models in simulating the material behaviour is considered.

A challenging aspect of the software used in modelling cast iron pipes material is its limited material constitutive models. Unlike steel, cast iron is a material which has different mechanical properties and stress-strain behaviour in tension and compression. The software should thus have the capability to support user-modified material models.

Thirdly, the software should have a user-friendly interface. Powerful pre- and post-processing capabilities such as geometry and mesh creation as well as the ease of output data processing were taken into account.

Two types of commercially available finite element software, ANSYS and ABAQUS, were assessed. ABAQUS was chosen because its features allow non-linear material behaviour to be modeled easily (Pike 2016).

4.3 Numerical Modelling of Flat Specimen in Tension

As discussed in Chapter 3, eleven flat specimens were removed from a cast iron pipe and were tested under axial tension. The nominal sizes of the specimens were the same. Therefore, a typical specimen was modelled for finite element analysis. One of the tests was simulated and the results were compared.

In all of the tests conducted, failure occurred near or the top of the gauge section as shown in Figure 4-2. Finite element analysis was used to explain the failure mechanism observed.

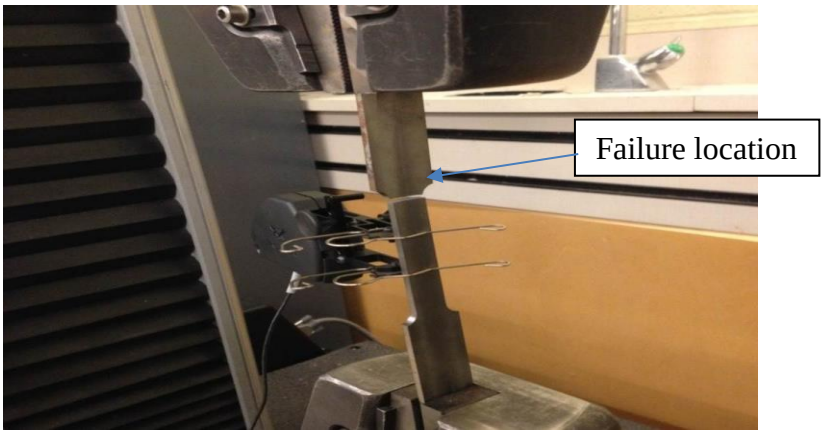

Figure 4-2: The fracture occurred at the top of the gauge section

4.3.1 Modeling of the Test Specimen

Figure 4-3 shows the idealization of the tensile test specimen. Actual geometry of test specimen was modelled (Figure 4-3a). Eight-nodded three dimensional continuum elements (ABAQUS element "C3D8R") are used to discretize the model. A mesh sensitivity analysis was conducted to determine the element size in finite element mesh since mesh size is expected to influence the results due to the non linear stress distribution within the sample. The final element size for meshing the test specimen is 0.0039 m.

The boundary and loading conditions of the test are as follows. One end of the test specimen is fixed and therefore prevented from displacing or rotating in the x, y, and z directions. The other end is subjected to slowly increasing tension. Static

analysis was conducted. The finite element model information is provided in Table 4.1.

Table 4.1: Summary of finite element model

Geometry	
Length of Flat Specimen	229 mm
Thickness of Flat Specimen	3.18 mm
Width 1 of Flat Specimen (Figure 4-3b)	22 mm
Width 2 of Flat Specimen	12.7 mm
Radius at the intersection	6.35 mm
Meshing	
Number of nodes	854
Number of elements	360

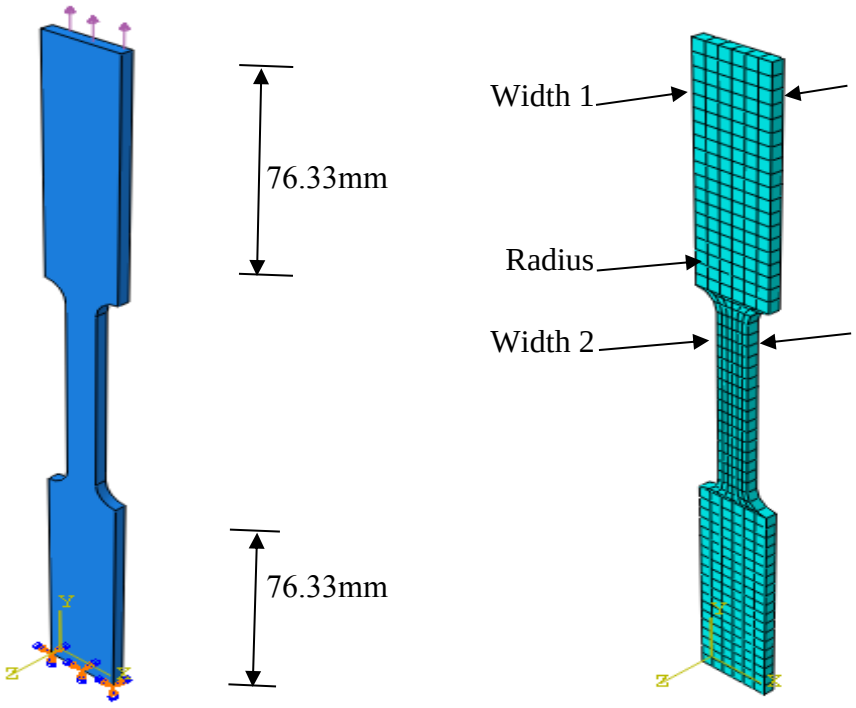

(a) Model Specimen (b) FE Mesh

Figure 4-3: Finite Element modelling of tensile test specimen

A linear elastic material model was first used. Material parameters were: Young's modulus of 150 GPa and Poisson's ratio of 0.27. Analysis with a non-linear material model was also performed. In the non-linear material model, the stresses and corresponding plastic strains were provided beyond a linear-elastic yield point. The plastic strains were calculated using following equation:

$$\varepsilon_{pl} = \varepsilon_{tru} - \frac{\sigma_{tru}}{E_i} \quad (4\text{-}1)$$

Where

σ_{true} = True stress from experiment [MPa]

ε_{true}= True total strain from experiment

ε_{pl}= Plastic strain

E_i= Initial slope of the stress-strain curve (modulus of elasticity)

4.3.2 Results of Analysis

Figure 4-4 compares the stress-strain response from finite element analysis and the experiment for specimen No. 5 randomly. Material parameters obtained from experiments were used in the finite element analysis. In Figure 4-4, experimental measurements match perfectly with those calculated using finite element analysis. The finite element model thus reasonably simulates the test conditions.

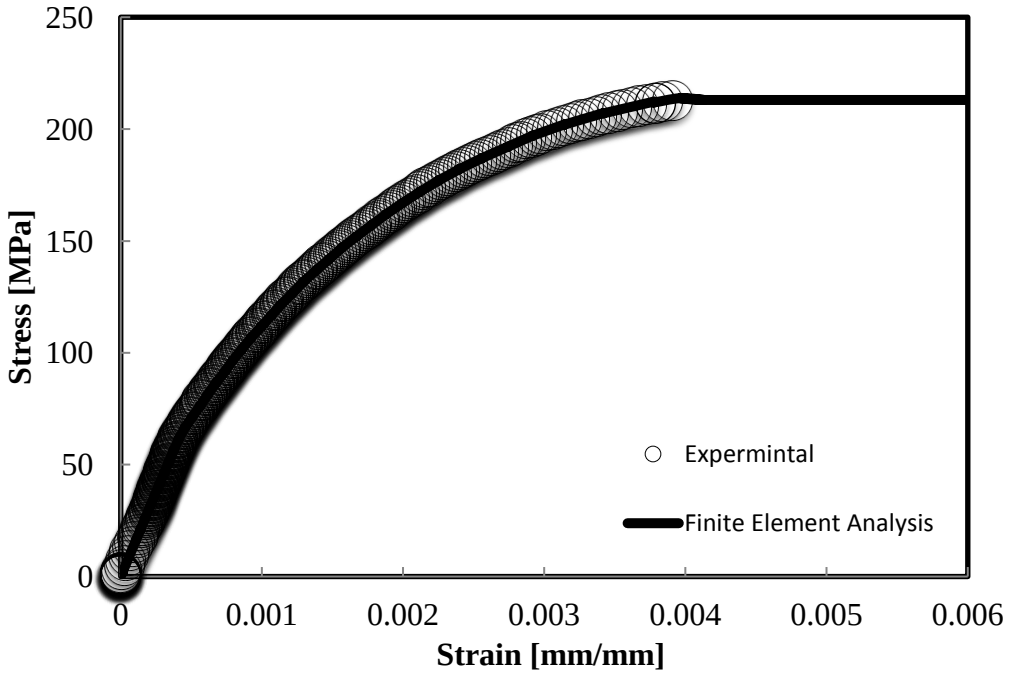

Figure 4-4: Comparison of stress-strain relations for a Tensile test

Figure 4-5 shows the contour of major principal stress at a tensile load of 9 KN. The figure reveals that a concentration of stress occurs within the curved zone near the change in the cross-section of the specimen. The stress in the curve zone is about 26 times the stress at the mid-span of the specimen. Since cast iron is brittle material, high stress may lead to crack initiation that propagates up to the failure of the specimen at this point. Thus, the ultimate tensile strength obtained from the test is expected to be less than the strength of a specimen in pure tension. It is therefore recommended to use different specimen shapes for tensile tests of cast iron.

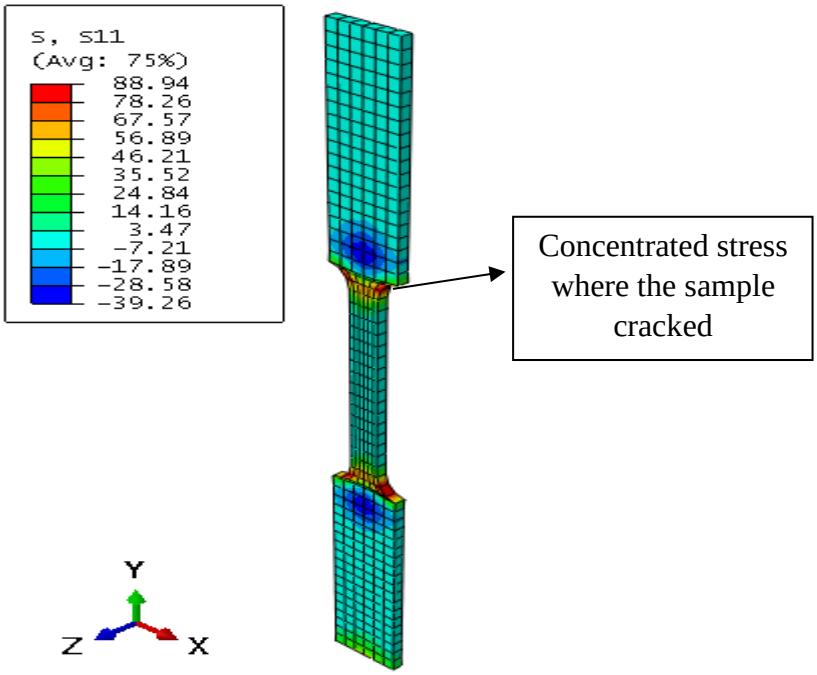

Figure 4-5: Stress concentration shows at the top of the gauge section

4.4 Modelling on Single-Edge Notched Beam Test

Single-Edge Notched Beam (SENB) tests were conducted with different depths of the notches. Each of these tests were modelled. Figure 4-6 shows a typical finite element idealization of an SENB test. A simply supported beam with a notch is modelled using the finite element method. Point load is applied using an assembly as shown in Figure 4-6(a).

Meshing plays an important role in modelling the notched beam using the finite element method. The notch causes non-linearity of stress that cannot be captured using coarse mesh. On the other hand, if the mesh is too fine, the computational time would be significantly high. A mesh sensitivity study was conducted by modifying the size of each element, running the analysis and comparing the results to observe if the

stresses change with the changes in element sizes. This was continued until there was no large changes in the stresses. The finite element meshes thus obtained for notch depths of 3.2 mm, 4.7 mm, 6 mm, and 7.5 mm are shown in Figure 4-7, Figure 4-8, Figure 4-9, and Figure 4-10, respectively.

Boundary conditions were selected for simply supported beams. End supports were provided at the bottom. An assembly at the middle of the span was subjected to a concentrated load as it was applied during the tests.

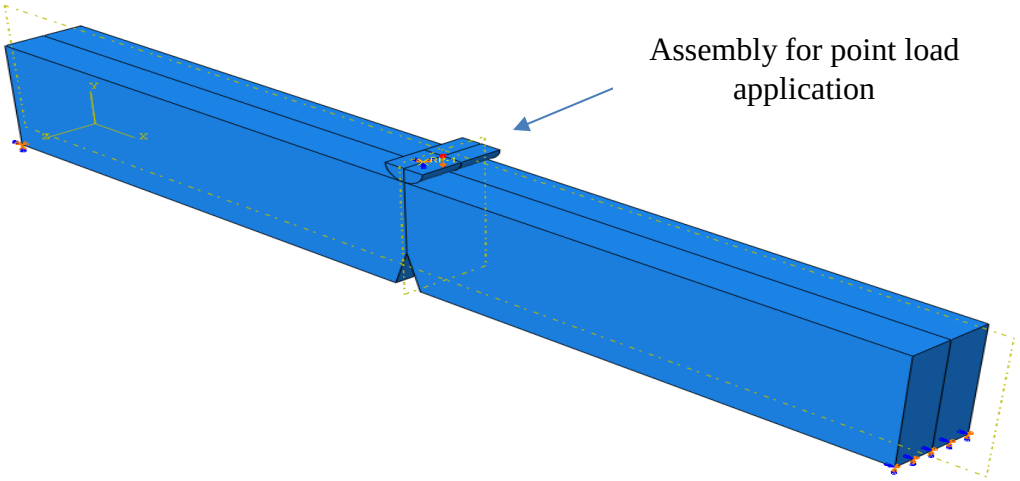

(a) Idealization

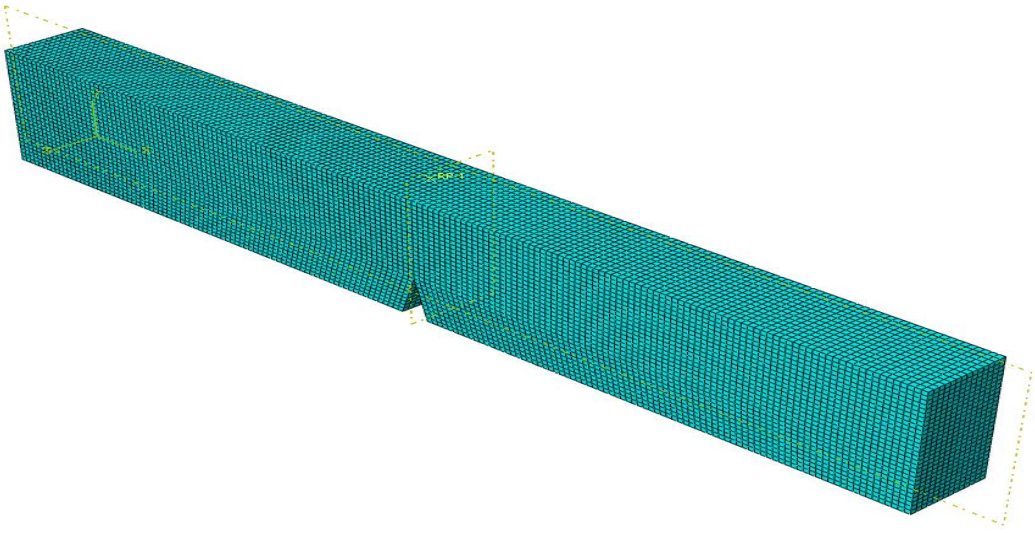

(b) FE mesh

Figure 4-6: A Typical FE Model of SENB Test

The grey cast iron material properties are provided to represent the linear elastic material behavior. The three elastic material parameters are: Young's Modulus, Density, and Poisson's Ratio.

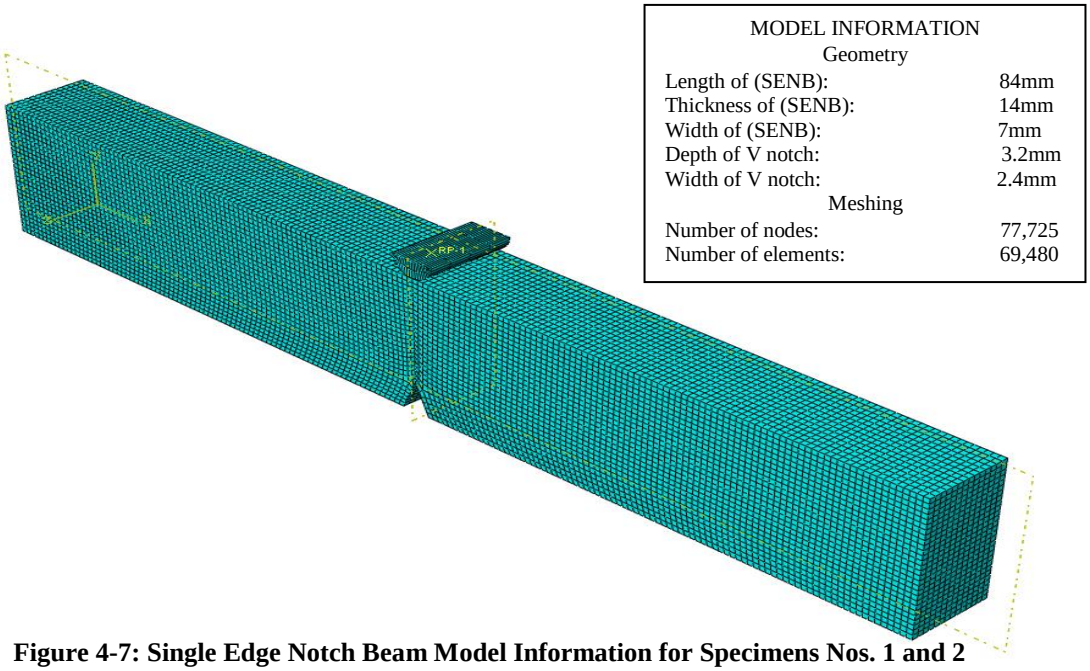

Figure 4-7: Single Edge Notch Beam Model Information for Specimens Nos. 1 and 2

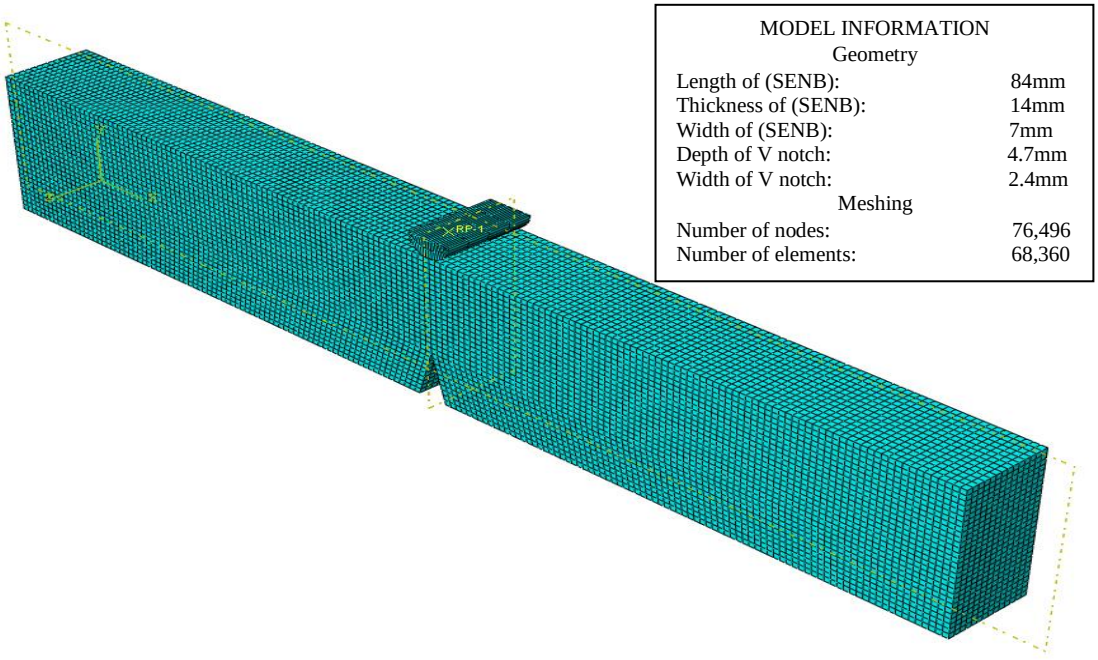

Figure 4-8: Single Edge Notch Beam Model Information for Specimens Nos. 3, 4, 5 and 6

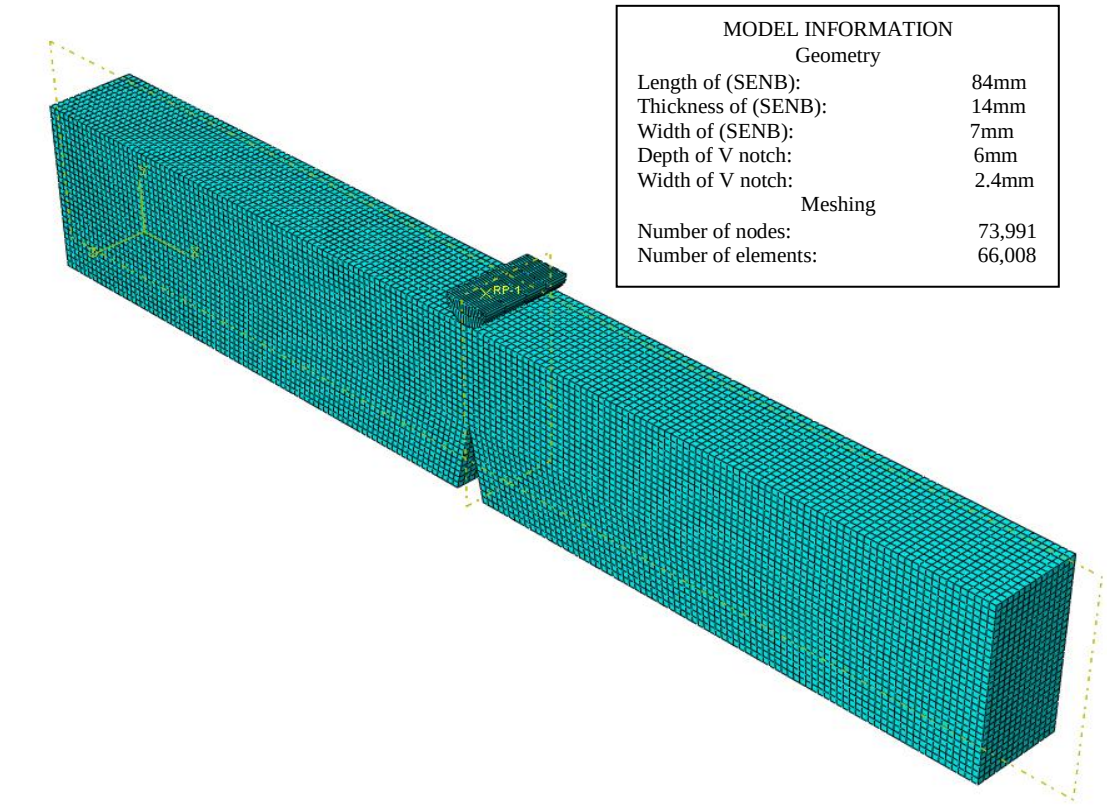

Figure 4-9: Single Edge Notch Beam Model Information for Specimens Nos. 7 and 8

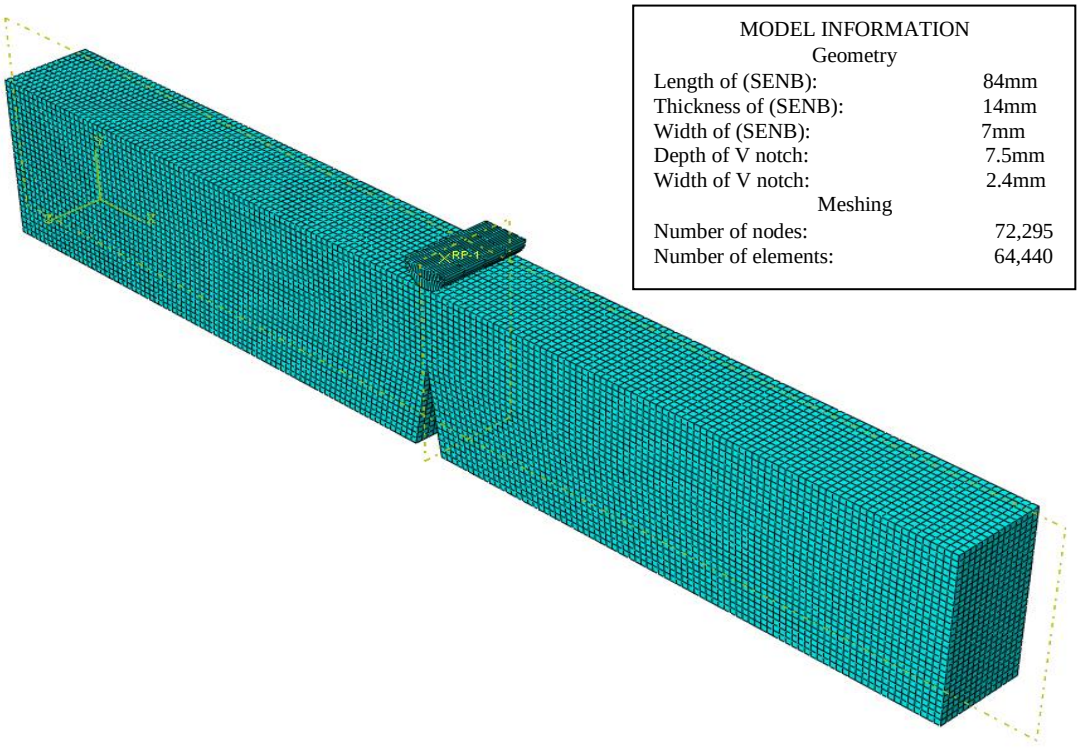

Figure 4-10: Single Edge Notch Beam Model Information for Specimens Nos. 9 and 10

4.4.1 Results of Analysis

Linear-elastic analyses were performed using a back-calculated elastic modulus, as is discussed in Chapter 3. The modulus was computed assuming the deflection equation for a simply supported beam. In this equation, the effect of the notch was neglected. The slope of the secant line to the load-displacement curve was employed instead of the slope of the initial tangent line. This is because the load-displacement curves were semi-linear. The secant line is used to obtain an averaged stiffness along the load-displacement curve as opposed to the slope of a tangent at a point on the curve, which would provide an initial "instantaneous" value.

Finite element analysis was conducted on the beam without the notch, the beam with a depth up to the tip of the notch, and the beam with the notch as shown in Figure 4-11, Figure 4-12, and Figure 4-13, respectively. The load-displacement graph that was derived from linear-elastic finite element analyses is shown in Figure 4-14. The calculated load-displacement response is compared with the load-displacement response obtained from experiments in the figure. In Figure 4-14, the response with the beam with the V-notch is located between the responses without the notch with full-depth of the beam and with the depth up to the tip of the notch, as expected. However, the responses are far from each other, indicating that simplified idealization neglecting the notch cannot be used for analysis of a beam with a notch. Therefore, the modulus of elasticity calculated in Chapter 3 for SENB tests without consideration of the notch is expected to be erroneous. As a result, the response calculated from finite element analysis is different from the response obtained from the test (Figure 4-14). Finite element analysis was then conducted with different values of the Young's modulus of the material to obtain a modulus of elasticity that provides a response

close to those obtained from the tests. The modulus of elasticity thus obtained is summarized in Table 4.3. The modulus of elasticity ranges from about 120 GPa to 280 GPa. The estimated resulting load-displacement responses are compared in Figure 4-15 to 4-24. It should be noted that the load-displacement response from SENB tests are almost linear with the finite element calculation, matching the experimental measurement reasonably. The non-linear load-displacement response was observed in Test No 10, with the highest depth of the notch being 7.5 mm. However, the initial portion of the response is linear, while demonstrating a ductile behaviour beyond that.

Table 4.2: Parameters estimated for SENB Tests

Test #	Depth of notch (a) mm	Failure Force P [N]	Failure Displacement	Estimated Modulus of elasticity [GPa]
SB1	3.2	1869	0.17	121
SB2	3.2	2106	0.19	131
SB3	4.7	1191	0.12	118
SB4	4.7	1068	0.12	118
SB5	4.7	1020	0.12	122
SB6	4.7	1523	0.14	160
SB7	6	1179	0.13	180
SB8	6	1136	0.11	195
SB9	7.5	939	0.12	218
SB10	7.5	816	0.13	280

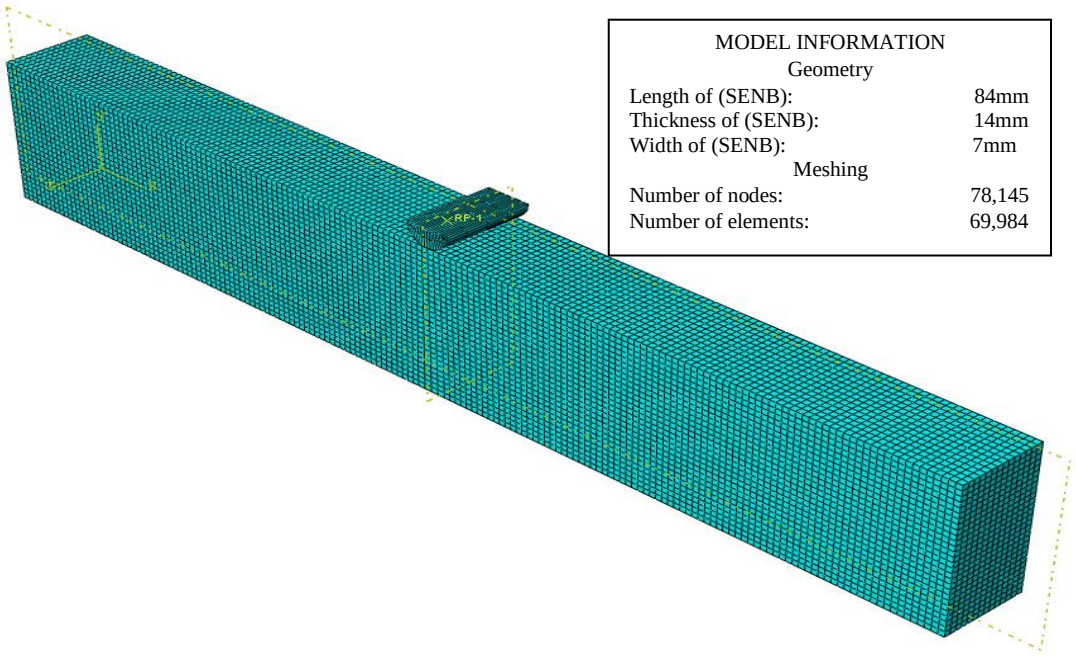

Figure 4-11: FE Model Information of beam with full depth

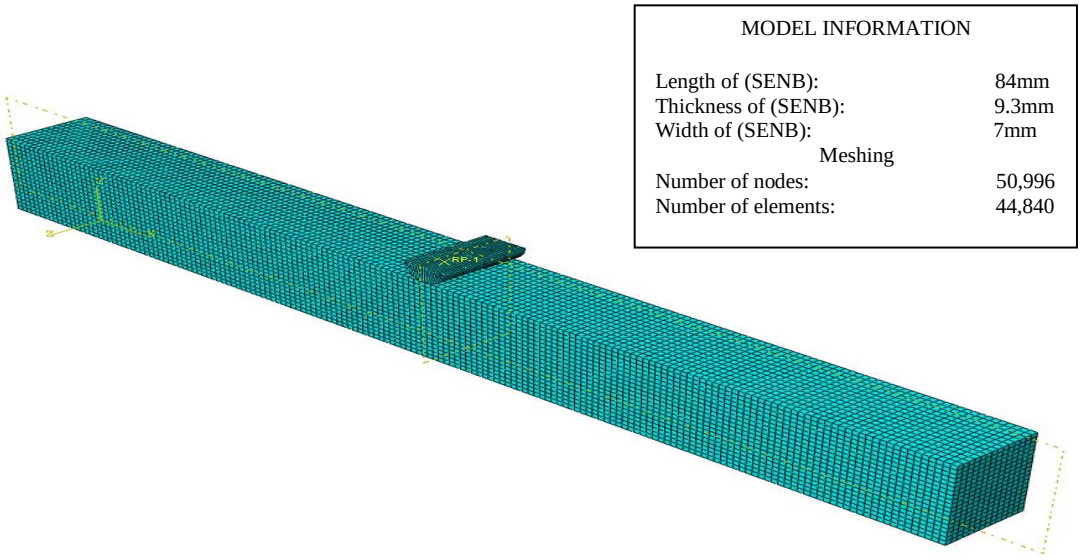

Figure 4-12: FE Model Information of beam with depth up to the tip of notch

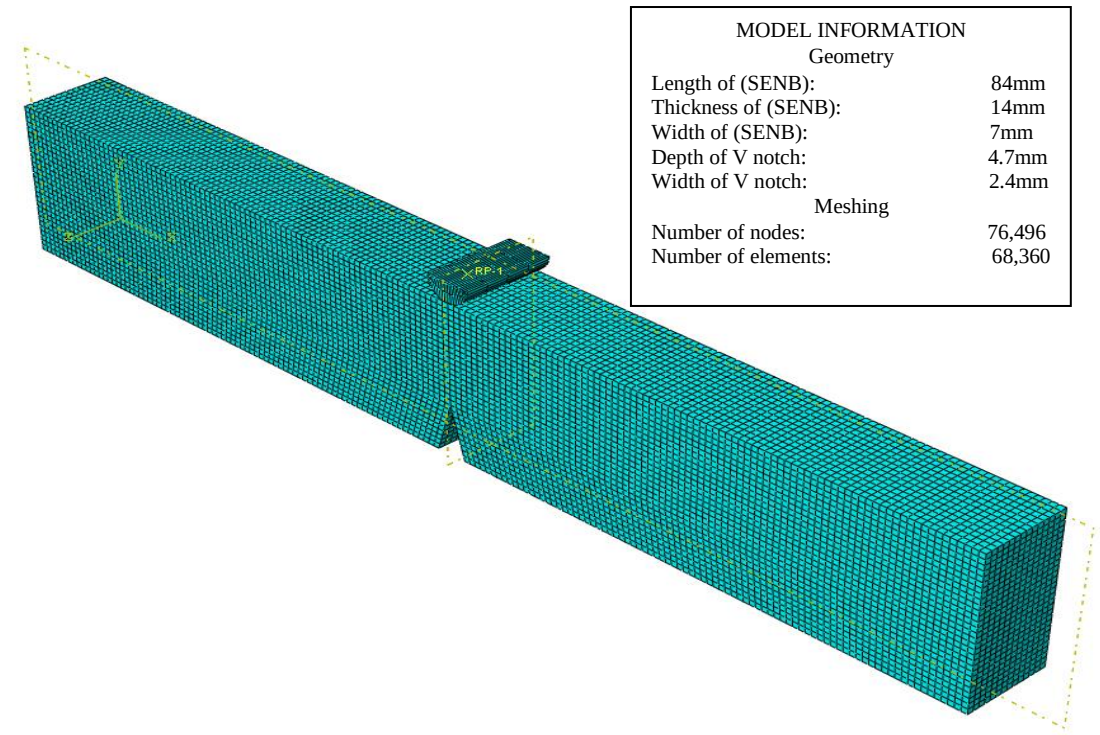

Figure 4-13: FE Model Information of beam with a V-notch

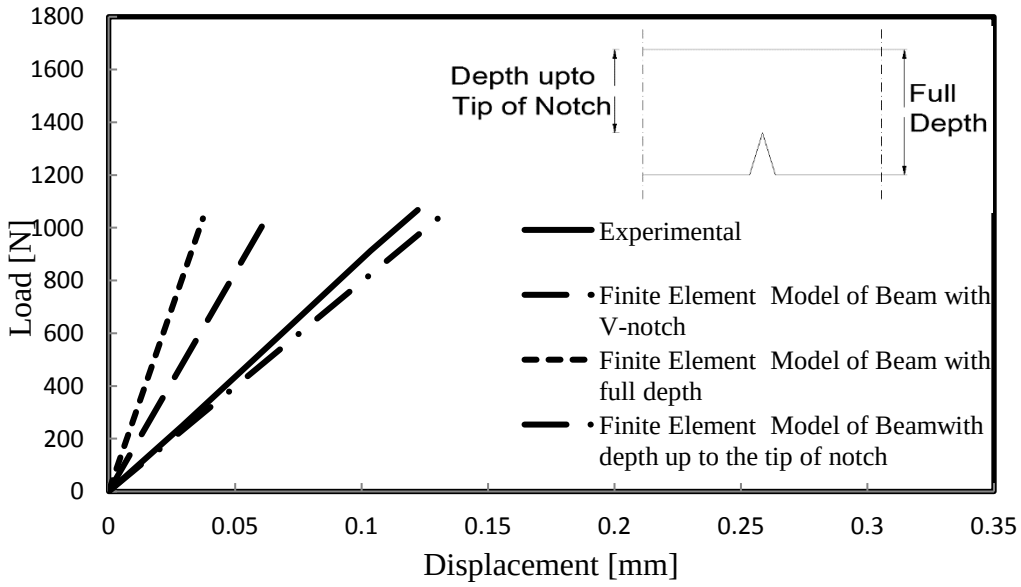

Figure 4-14: Load-Displacement Response

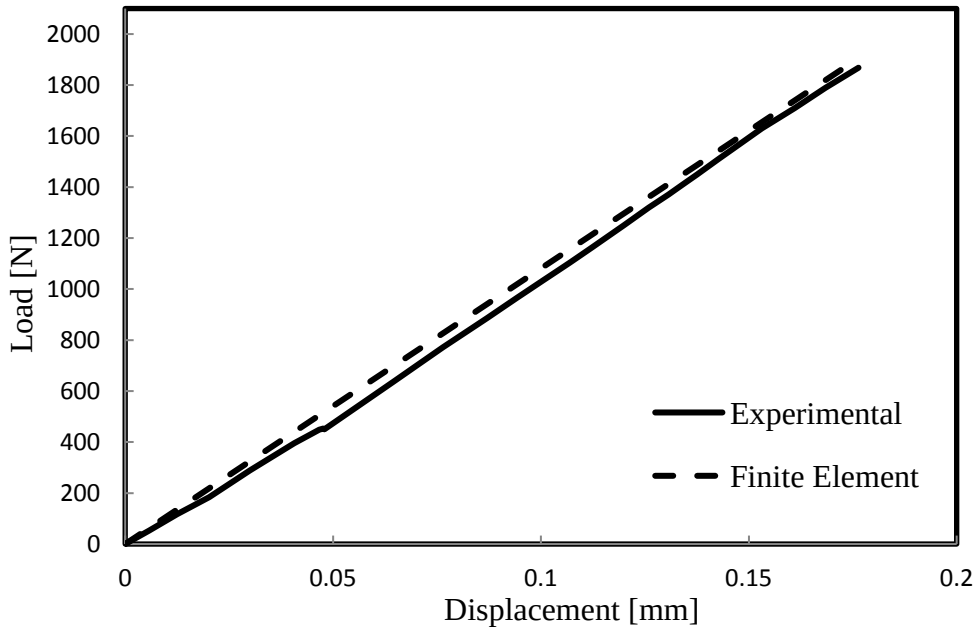

Figure 4-15: Load-Displacement Response for Single Edge Notch Beam Test (Test No. SB1)

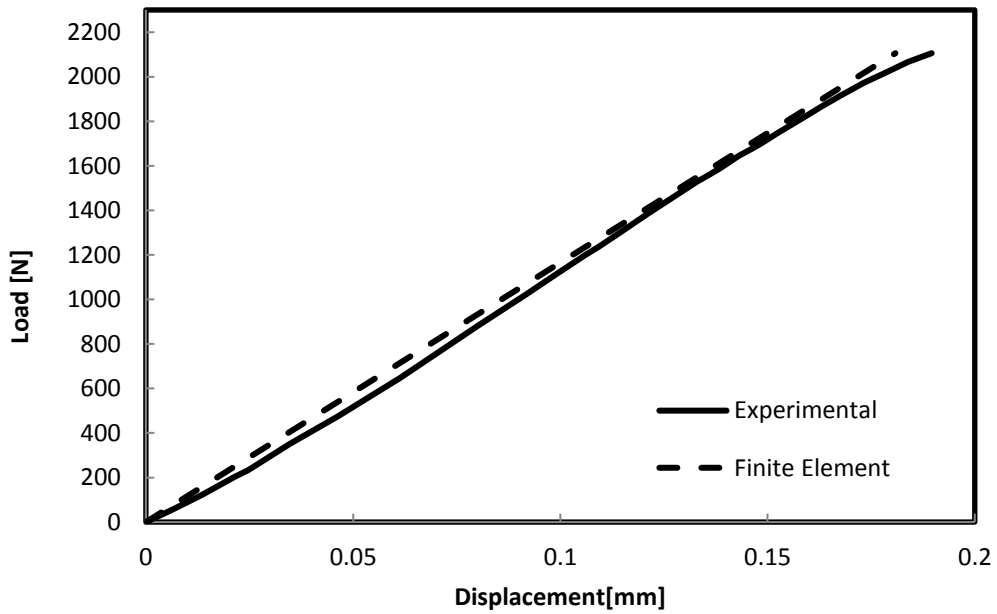

Figure 4-16: Load-Displacement Response for Single Edge Notch Beam Test (Test No. SB2)

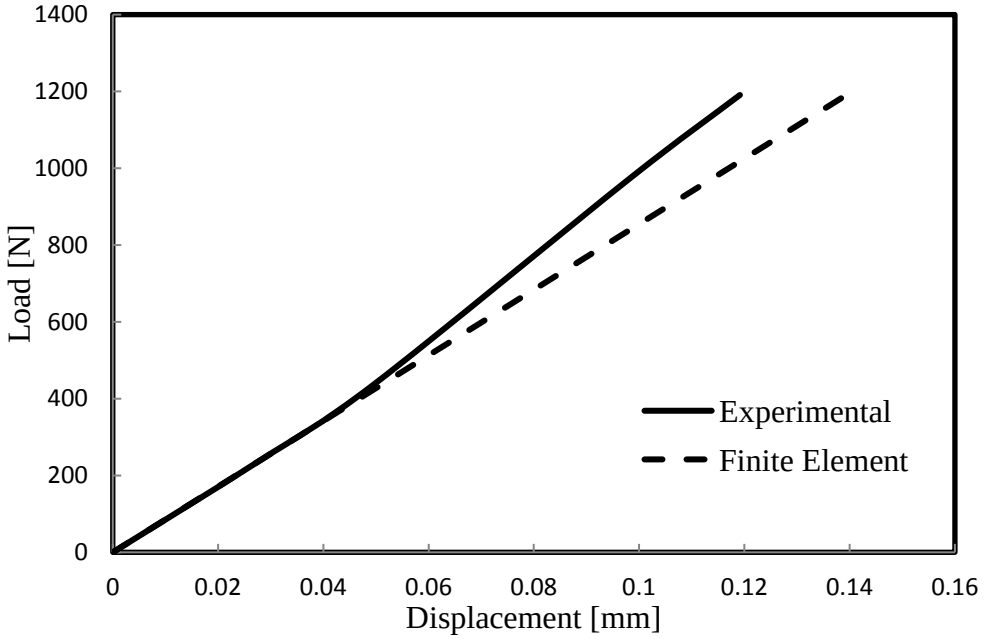

Figure 4-17: Load-Displacement Response for Single Edge Notch Beam Test (Test No. SB3)

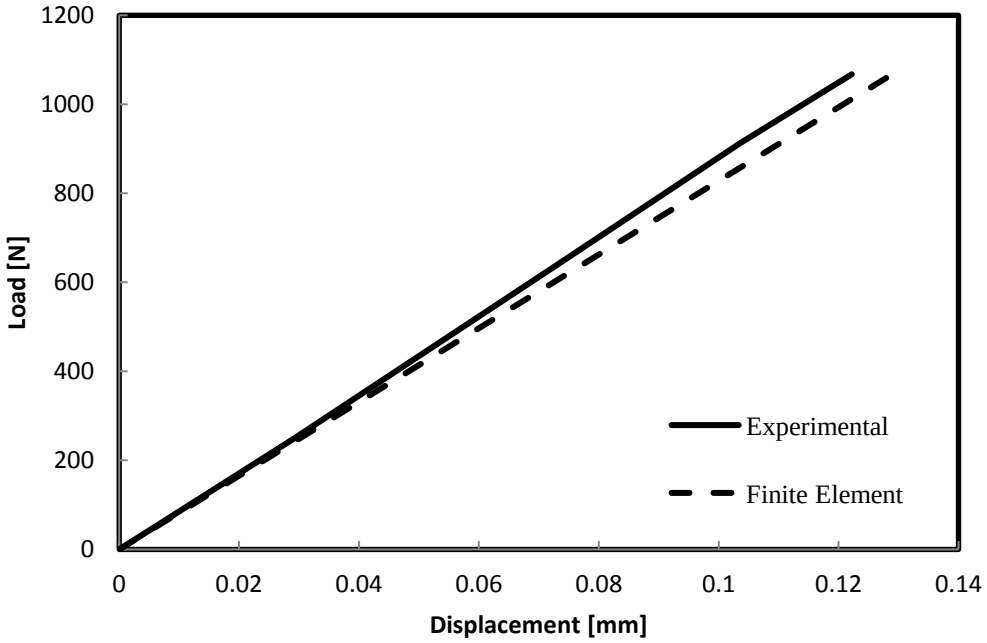

Figure 4-18: Load-Displacement Response for Single Edge Notch Beam Test (Test No. SB4)

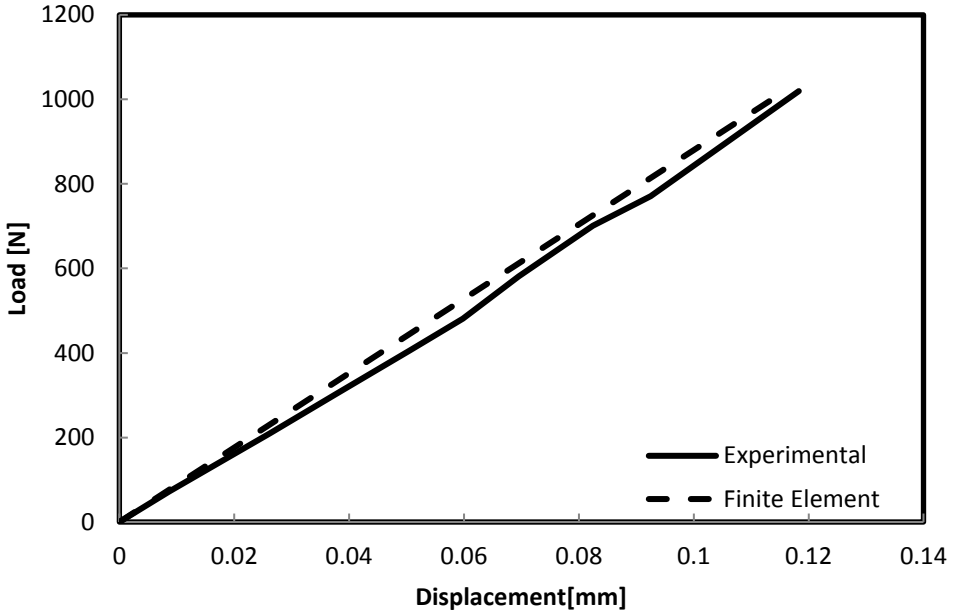

Figure 4-19: Load-Displacement Response for Single Edge Notch Beam Test (Test No. SB5)

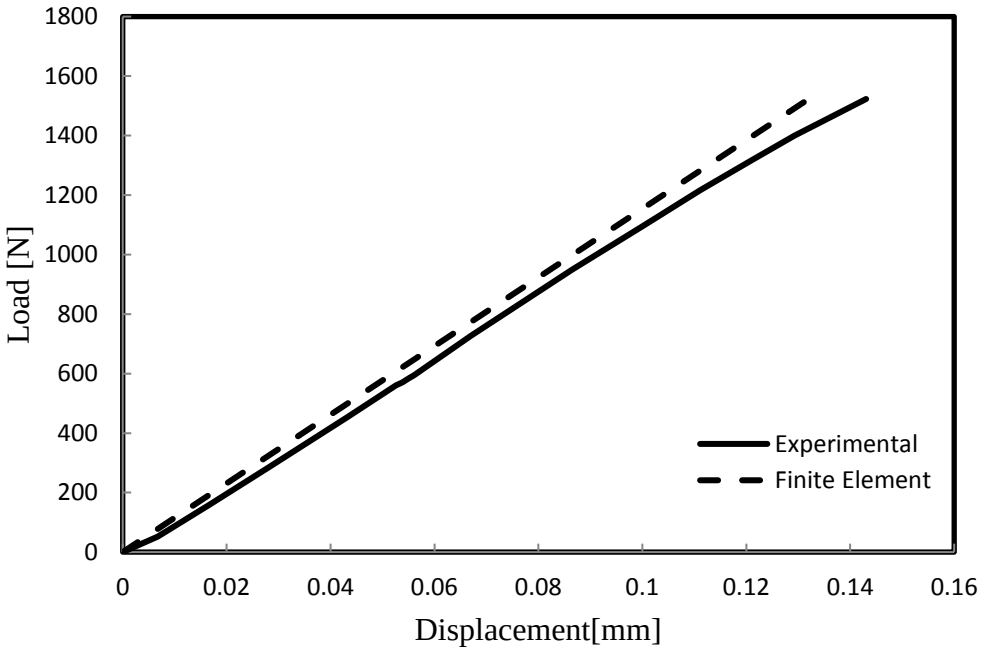

Figure 4- 20: Load-Displacement Response for Single Edge Notch Beam Test (Test No. SB6)

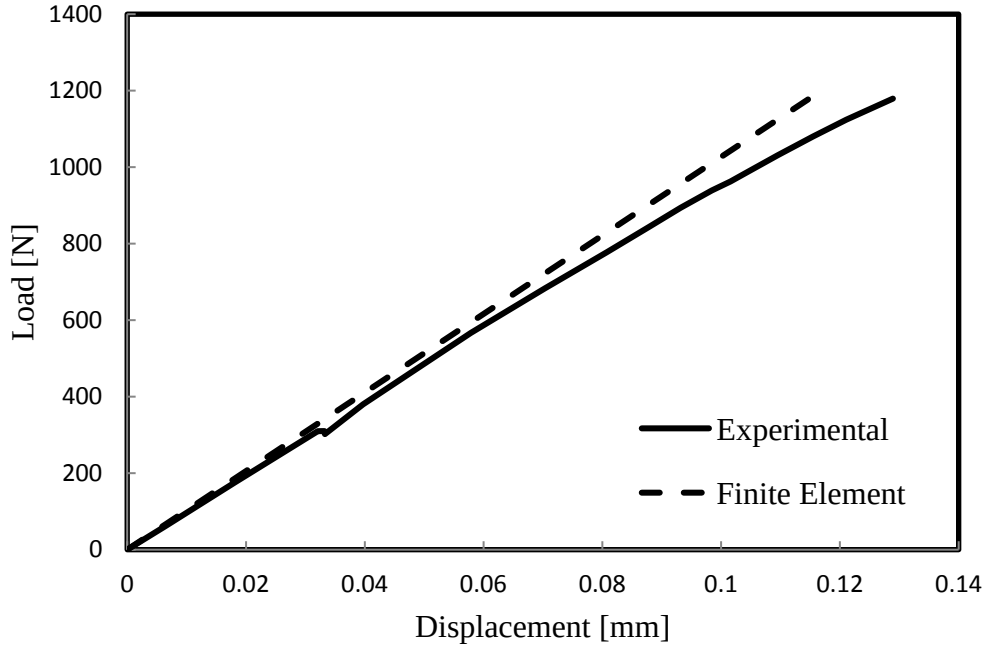

Figure 4-21: Load-Displacement Response for Single Edge Notch Beam Test (Test No. SB7)

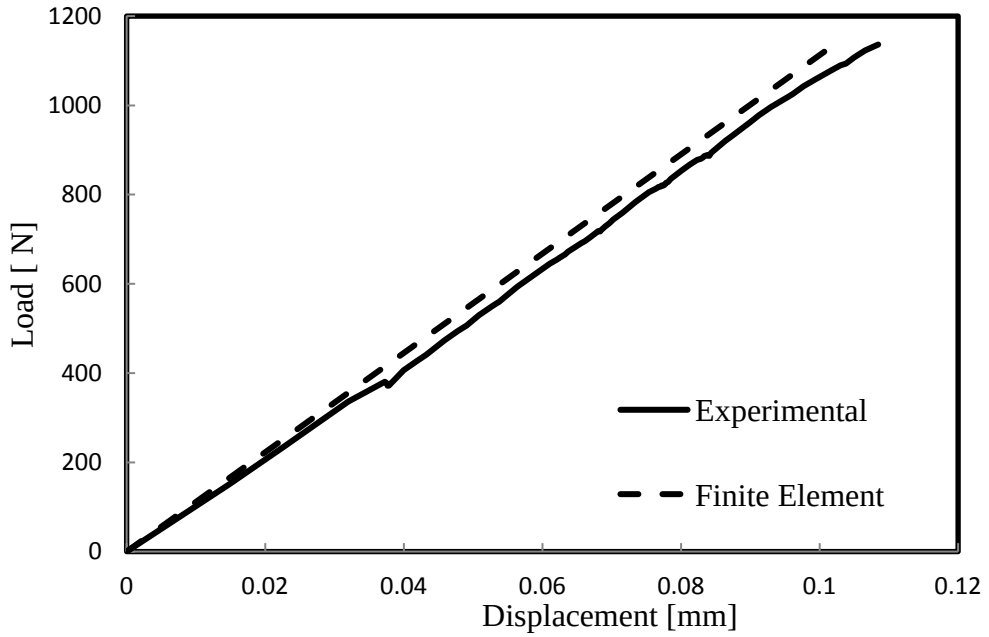

Figure 4-22: Load-Displacement Response for Single Edge Notch Beam Test (Test No. SB8)

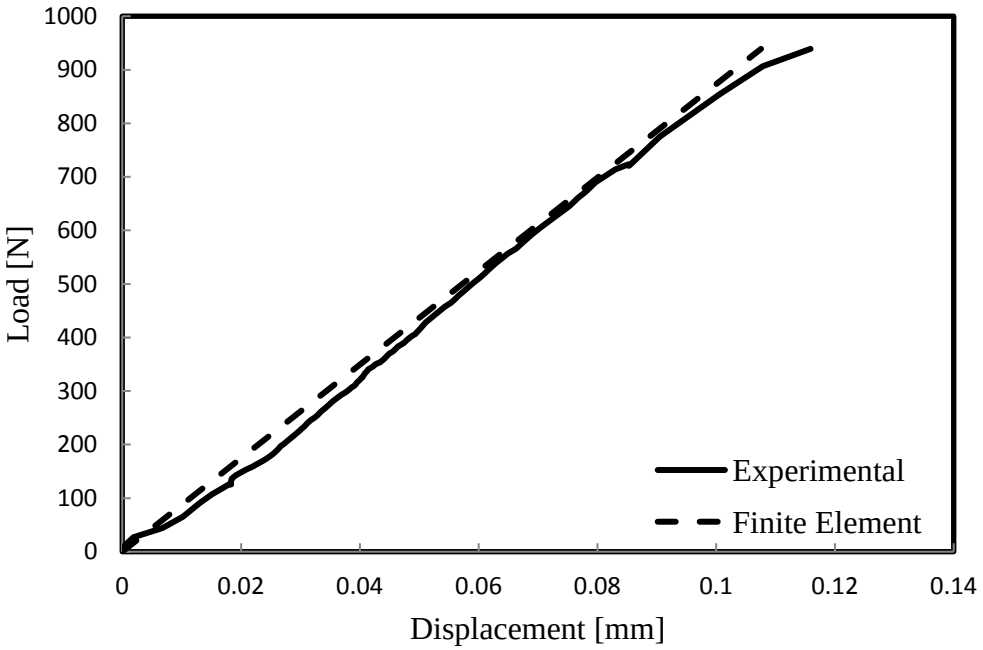

Figure 4-23: Load-Displacement Response for Single Edge Notch Beam Test (Test No. SB9)

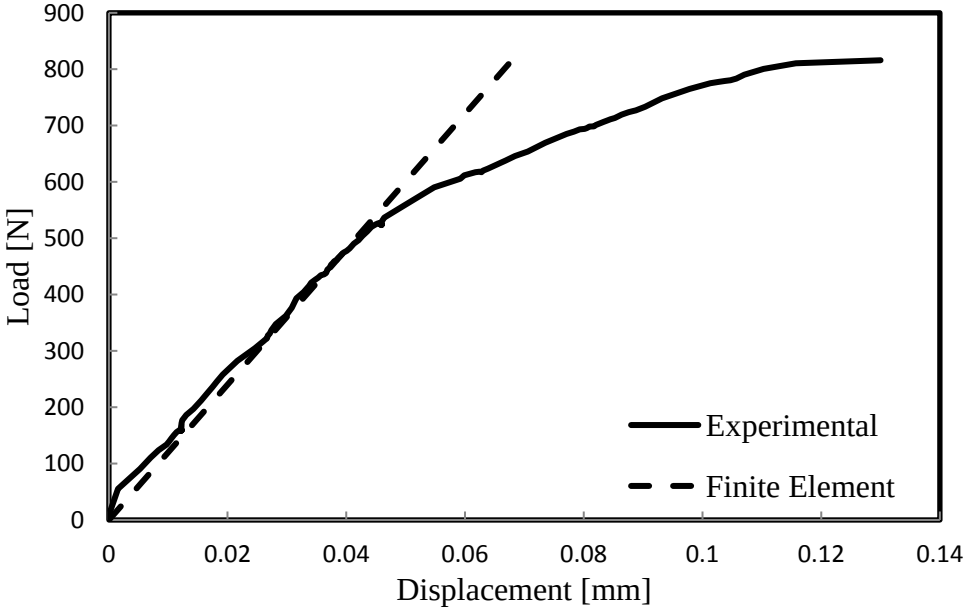

Figure 4-24: Load-Displacement Response for Single Edge Notch Beam Test (Test No. SB10)

To demonstrate the bending deformation of the cross-section, the axial strain throughout the depth of the beam is examined at the mid-length of the beam. Figure 4-25 plots the variation of axial strain with depth. Axial strains calculated using the finite element method and those obtained from the measurements during the tests are compared in the figure. In Figure 4-25, experimental strains match with the calculations using the finite element method, indicating that the finite element model reasonably simulates the test conditions.

Figure 4-25 reveals that the point of zero strain (neutral axis) is located at a distance of 6 mm from the top of the beam. The centroid of the cross-section (mid-depth) is located at 4.65 mm from the top. Thus, the neutral axis is somewhat different from the centroidal axis. The presence of a notch appears to affect the bending mechanism that cannot be captured using classical beam theory but can reasonably be captured using FE analysis. The conditions of classified beam theory (such as plane section remain plane) are not satisfied here. The strains near the notch are significantly increased.

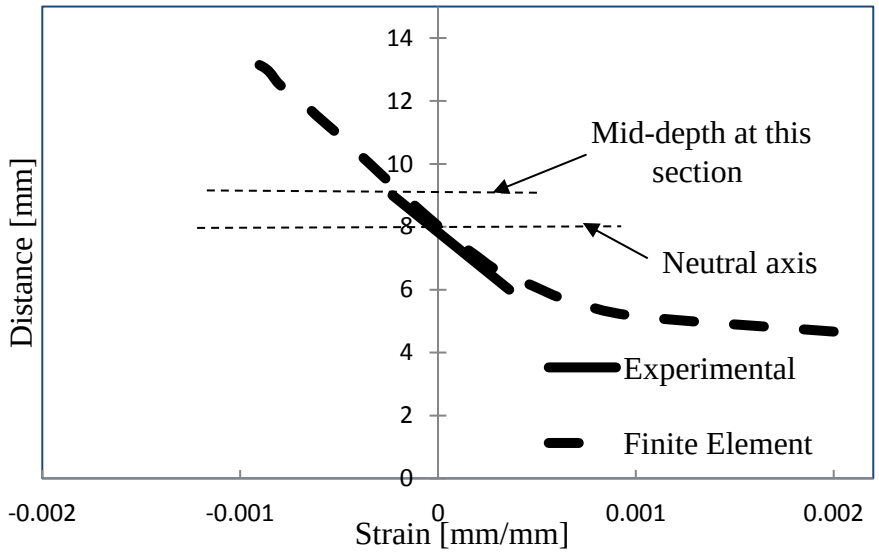

Figure 4-25: Strain-Distance Graphs for Test No. 4, Load=1068 N, notch depth= 4.7 mm

It appears from Figure 4-25 that the neutral axis moves towards the tension side during bending. This is due to the concentration of stress because of the notch. For a uniform beam, the neutral axis moves toward the compression side for the cast iron beam (Shawki and Naga., 1986).

Figure 4-26 shows the contour of major principle stress for the beam in a SENB test. The contour is plotted at a load of 514 N. The notch depth of the beam is 7.5 mm. At this load, the non-linearity in the load-displacement response starts.

Stress concentration at the tip of the notch is developed (Figure 4-26). The magnitude of the highest stress is 195 MPa, which is close to the estimated yield stress of the material. The maximum stresses at the failure loads in tests Nos. 1, 2, 3, 4, 5, 6, 7, 8, 9, and 10 are 446 MPa, 500 MPa, 300 MPa, 286 MPa, 260 MPa, 388 MPa, 374 MPa, 360 MPa, 406 MPa, and 353 MPa, respectively. The maximum stresses at the failure loads are thus different in different tests, which are higher than the tensile strength of the material. The higher tensile strengths in bending (higher modulus of rupture) for cast iron were reported earlier in Seica (2002).

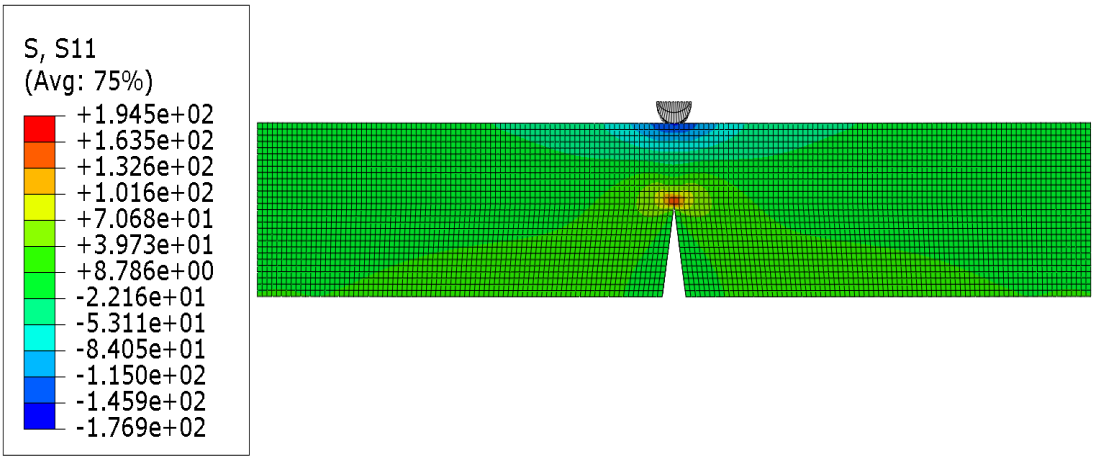

Figure 4-26: Contour of Major Principle for Test No 10 at Load 514N

Chapter 5: Conclusion and Recommendations for future studies

5.1 Introduction

Many possible factors may be directly or indirectly involved in water main failure. Experience has revealed that the most common cause of cast iron pipe failure is a mixture of corrosion and mechanical actions. Other factors which contribute significantly to pipe failure include casting technology, manufacturing defects, and specific local conditions.

Understanding the failure mechanism of cast iron water mains is the major focus of this research. The research commences with the physical examination of a cast iron water main exhumed from the city of Mount Pearl to determine and estimate the condition of deterioration.

Specimens extracted from the exhumed pipe sample were tested to determine the mechanical properties. Mechanical tests included tensile tests and Single-Edge Notched Beam (SENB) tests. Eleven samples were tested under axial tension. Ten samples were tested in SENB bending.

The experimental tests were then analysed using the finite element method (FEM). Commercially-available software (viz. ABAQUS) was used to model the specimens in tensile tests and single-edge notched bend (SENB) tests. The results of the finite element method were then compared with the experimental results and the results were found to be in accordance with one another. One result of this study has

been that the mechanical strength of pipes can be evaluated using numerical modelling to assess structural integrity.

The study reveals that the properties of cast iron may not change significantly during the service life; however, material parameters appear to vary for the same pipe component. The results from this thesis will be useful for utility companies in assessing the structural condition of infrastructure. Such pipes need to be identified. On the other hand, some pipes may be subjected to higher-than-anticipated loads in certain select locations and, as a result, the pipes may fail. Therefore, it is of the utmost importance to understand the mechanical properties of cast iron pipes in a particular distribution system. A better understanding of pipe failure mechanisms can lead to a realistic evaluation of the strength of the pipes in the system, and hence of their current level of safety.

The findings from the experimental and numerical study conducted in this research are summarized below.

5.2 Laboratory investigation

Factors influencing the pipe failure include corrosion, manufacturing defects, and the tensile strength of the material. Corrosion can affect the strength of the pipe material by causing stress concentration and crack initiation. Physical examination of the pipe sample indicates that the effect of corrosion is significant on the outer surface of the pipe. Manufacturing defects were encountered on the inner surface. The corrosion and the manufacturing defects can influence the strength of the pipe material. This type of defect may lead to subcritical crack growth in the pipe wall. Tests on flat specimens were performed to determine the tensile strength of the cast

iron material. Dogbone-shaped specimens were prepared and tested. All specimens failed near the interface at the change of the cross-sectional area of the sample, indicating that the measured strength is not the true ultimate strength of the material. The stress-strain responses were found to depend on the loading rate and were stiffer for higher loading rates. The initial slope of the stress-strain response and ultimate tensile strength were found to be higher for higher loading rates. For a loading rate (deformation rate) of 20 mm/min, the initial modulus varied from 98 GPa to 185 GPa and the ultimate tensile strength varied from 184 MPa to 195 MPa. For a loading rate of 0.5 mm/min, the initial modulus and ultimate strength were 69 GPa and 163 MPa, respectively. However, the ultimate strength of the material was not found to vary significantly with the rate of loading. The ultimate strengths for the sample varied from around 150 MPa to around 200 MPa. The failure strain at the ultimate strength varied from 0.002 to 0.005.

The Poisson's ratio for the cast iron pipe material was also measured through measurement of longitudinal and lateral strains. The Poisson's ratio ranged from 0.22 to 0.34.

The loading-unloading-reloading behaviour examined during the tests indicates that the unloading-reloading line is parallel to the initial straight line within the tension zone; however, the response was stiffer within the compression zone.

Hardness tests were performed at different locations on the flat specimen. However, all values which were computed from the Rockwell hardness tests were in accordance to the maximum average hardness values in standard specifications (AWWA 1975).

SENB tests used to determine fracture toughness were conducted with specimens extracted from the exhumed pipe. Fracture toughness is a measure of crack propagation that has a range of values depending on the details of the microstructure of the material. The fracture toughness generally varies with the length of the crack, defect sizes, temperature, case of stress levels, and strain-rate. All these fractures can lead to the structural failure of water mains.

To assess the pipe line condition, a thorough investigation of a pipe can be performed in order to provide an understanding of the effects of defects. In this regard, the relationship between the amount of material loss and the pipe fail can be developed. The year the pipe was produced can give a good indication of the technology and the manufacturing process was used for the pipe. Based on this indication, an assessment using the mechanical properties of the pipe material can be performed. The mechanical properties in the bending and fracture toughness of cast iron pipe material are investigated. The measurement of strain in tension and compression implied that stress-strain behaviour is non-linear in tension and linear in compression. The presence of a notch appeared to cause stress concentration near the tip that shifted the neutral axis. As a result, the strain at the mid-depth of the beam was not zero. The stress intensity factors calculated from the test results ranged from 4.75 $N/mm^{3/2}$ to 12 $N/mm^{3/2}$.

5.3 Finite Element Modelling

Finite element analysis of the tests provided an understanding of the mechanism of the stress-deformation behaviour during the tests. Finite element analysis with non-linear stress-strain behaviour reasonably simulated the load-

deformation response in the tensile tests. For SENB tests, a linear model with a second modulus successfully simulated the load-deflection response.

Analyses of tensile tests reveals that stress concentration developed at the intersection of the cross-section in the dogbone-shaped specimen. A crack was thus initiated at the intersection that propagated to the failure of the specimen. Therefore, the tensile strength obtained from the tests is expected to be less than the true tensile strength of the material. It is therefore recommended not to use dogbone-shaped specimens for tensile tests of cast iron.

Analyses of SENB tests show that the presence of the notch affected the bending behaviour significantly. Thus, beam deflection cannot be calculated using classical beam theory while neglecting the effect of a notch. The modulus of elasticity calculated using the classical beam theory was found to be erroneous. Finite element analyses were conducted with different values of the modulus of elasticity to produce the laboratory test results. The modulus of elasticity thus estimated ranges from 120 GPa to 280 GPa.

Axial strains measured with beam depth match the bending strains calculated using the finite element analysis, indicating that the finite element model reasonably simulated the test conditions. The analysis and the experiments reveal that the point of zero-strain (neutral axis) is not at the mid-depth of the beam at the section, which is contrary to the classical beam theory. The neutral axis is shifted to below the mid-depth at the section of the notch, but above the mid-depth of the full-depth of the beam.

5.4 Recommendation

This research presents a study of the mechanical behavior of cast iron pipe material. Further study is recommended to complement the work completed in this research. The following presents a list of recommendations for future research:

Additional tensile tests should be conducted to extend the database for assessment of the variability of the material properties under different strain rates. The existing literature lacks a database on stress/strain rate-dependent material parameters for cast iron. The study presented in this research indicates that cast iron may possess stress/strain-dependent material parameters.

In the current research, loading-unloading and reloading response within the tensile zone are investigated. It is recommended to carry out loading-unloading and reloading tests within both the tension and compression zone, as the pipe is expected to experience repeated loading in tension and compression. Behaviour of the material under tension and compression should be examined.

It is recommended to conduct finite element analysis based on fracture mechanics theory in order to evaluate the stress intensity factor and fracture toughness.

The stress-deformation behaviour of buried pipes should be investigated using the material parameters deformation in the current research, as well as those in the published literature.

References

• (AWWA). (1975). “Cast-iron pipe centrifugally cast in metal molds”, American Water Works Association,1975, C106-75.

• ASA/AWWA A21.2/C 102-62 (1962). “American Standard for Cast-Iron Pipe, Pit-Cast, for Water or Other Liquids”, American Water Works Association, New York.

• ASA/AWWA A21.6/C106-62 (1962a). “American Standard for Cast-Iron Pipe, Centrifugally Cast in Metal Molds, for Water or Other Liquids”, American Water Works Association, New York.

• ASA/AWWA A21.8/C 108-62 (1962b). “American Standard for Cast-Iron Pipe, Centrifugally Cast in Sand-Lined Molds, for Water or Other Liquids”, American Water Works Association, New York.

• ASA/AWWAC106-75 (AWWA 1975). “American Standard for Cast-Iron Pipe, Centrifugally Cast in Metal Molds, for Water or Other Liquids”, American Water Works Association, New York.

• ASTM E18−15 (2015). “Standard Test Methods for Rockwell Hardness of Metallic Materials”, American Society for Testing and Materials, 2015.

•ASTM E8 /E8M –15(2015). “Standard Test Methods for Tension Testing of Metallic Materials”, American Society for Testing and Materials, Philadelphia, Pennsylvania.

• ASTM E1820-01(2001). “Standard Test Methods for Measurement of Fracture Toughness”, American Society for Testing and Materials, 2001 (03.01).

• Babbitt, H.E., Doland, J.J., Cleasby, J.L. (1962). “Water Supply Engineering", 6th Edition, McGraw-Hill.

• Bauld, N. R. (1986). “Mechanics of materials”, PWS Publishers, Boston, Mass.

• Belmonte, H. M. S., Mulheron, M. J., and Smith, P. A. (2009). “Some observations on the strength and fatigue properties of samples extracted from cast iron water mains.” Fatigue Fracture Eng. Mater. Struct., 32(11), 916–925.

• Caproco Corrosion Prevention Ltd. (1985). “Underground corrosion of water pipes in Canadian cities”, Case: The city of Calgary, Rep. Prepared for CANMET, Ottawa.

• CIPRA (1967). “Handbook of Cast Iron Pipe for Water, Gas, Sewerage, and Industrial Service”, Cast Iron Pipe Research Association, Chicago, Illinois.

• Conlin, R. M., and Baker, T. J. (1991). “Application of fracture mechanics to the failure behavior of buried cast iron mains”, Contract Rep. No. 266, Transport and Road Research Laboratory, London.

• CSCE. (1916). “Standard Specifications for Cast Iron Water Pipe and Special Castings”, Canadian Society for Civil Engineering, January.

• Cullin, M.J., Petersen, T.H. and Paris, A. (2014) “Corrosion Fatigue Failure of a Gray Cast Iron Water Main”, Journal of Pipeline Systems Engineering and Practice, ASCE, 2015 (6), 05014003-1-9.

• Folkman, S. (2012). "Water Main Break Rates in the USA and Canada: A Comprehensive Study." Utah State University, Logan, UT.

• Hjelm, H.E. (1994). “Yield Surface for Grey Cast Iron under Biaxial Stress”, Journal of Engineering Materials and Technology, vol. 116, no. 2, pp. 148-154.

• Jones, D. A. (1996). “Principles and prevention of corrosion”, 2nd Ed., Prentice Hall, Upper Saddle River, NJ.

• Josefson, B.L., Stigh, U., Hjelm, H.E. (1995). “A Nonlinear Kinematic Hardening Model for Elastoplastic Deformations in Grey Cast Iron” Journal of Engineering Materials and Technology, vol. 117, no. 2, pp. 145-150.

• Ma, Z., and Yamada, K. (1994). “Durability evaluation of cast iron water supply pipes by sampling tests” Proc., Structural Engineering, Japan Society of Civil Engineers, Tokyo, 40A.

• Makar, J. M., and McDonald, S. E. (2007). “Mechanical behavior of spun-cast gray iron pipe”, J. Mater. Civ. Eng., 826–833.

• Makar, J. M., Desnoyers, R., and McDonald, S. E. (2001). “Failure modes and mechanisms in gray cast iron pipe” Proc., Underground Infrastructure Research: Municipal, Industrial, and Environmental Applications, M. Knight, N. Thomson, eds., CRC, 1–10.

• Makar, J. M., Rogge, R., McDonald, S., and Tesfamariam, S. (2005). “The effect of corrosion pitting on circumferential failures in grey iron pipes”, American Water Works Association, Denver.

• Makar, J.M.; Rajani, B. (2000). “Grey Cast Iron Water Pipe Metallurgy”, Journal of Materials in Civil Engineering, vol. 12, no. 3, pp. 245-253.

• McGhee, T. J. (1991). “Water supply and sewerage”, 6th Ed., McGraw-Hill, New York.

• Mohebbi, H., Jesson, D.A., Mulheron, M.J., and Smith, P.A. (2010) “The fracture and fatigue properties of cast irons used for trunk mains in the water industry”, Materials Science and Engineering, 2010 (A527), 5915–5923

• Najafi, M., and Gokhale, S. (2005). Trenchless Technology: Pipeline and Utility Design, Construction and Renewal. McGraw-Hill, New York.

• Pike, K. (2016) “Physical And Numerical Modelling Of Pipe/Soil Interaction Events For Large Deformation Geohazards”, PhD Thesis, Faculty of Engineering and Applied Science, Memorial University of Newfoundland, St. John’s, NL, Canada.

• Rajani, B., and Kleiner, Y. (2010). “Fatigue failure of large-diameter cast iron mains”, Water distribution systems analysis, 1146–1159.

• Rajani, B., and McDonald, S. (1993). "Final Water Mains Break Data on Different Pipe Materials for 1992 and 1993." Rep. No. A-7019.1, National Research Council, Canada.

• Rajani, B.; Makar, J.M.; McDonald, S.E. (2001). “The Mechanical Properties of Grey Cast Iron Water Mains", Submitted for publication to the Journal of Materials in Civil Engineering.

• Seica, M.V. (2002). “Investigation of the Structural Performance of Cast Iron Water Pipes”, PhD Thesis, University of Toronto, Toronto, ON, Canada.

• Seica, M. V., and Packer, J. A. (2002). “Mechanical properties and strength of aged cast iron water pipes.” Journal of Materials in Civil Engineering. ASCE, 2004, (16), 69-77.

• Seica, M. V., and Packer, J. A. (2004). “Mechanical properties and strength of aged cast iron water pipes.” J. Mater. Civ. Eng., 69–77.

• Shawki, G. S. A., and Naga, S. A. R. (1986). “On the mechanics of gray cast iron under pure bending”, J. Eng. Mater. Technol., 108(2), 141–146.

• Stefanescu, D.M. (1990). “Classification and Basic Metallurgy of Cast Iron”, Metals Handbook, 10th Edition, Vol. 1: Properties and Selection: Irons, Steels, and High Performance Alloys, American Society for Metals, Metals Park, Ohio.

• USAS/AWWA A21.1/H1-67 (1967). “USA Standard for Thickness Design of Cast-Iron Pipe”, American Water Works Association, New York.

• Wang, G., Taylor, D., Bouquin, B., Devlukia, J. and Ciepalowicz, A. (2000). "Prediction of Fatigue Failure in a Camshaft Using the Crack Modelling Method", Engineering Failure Analysis, vol. 7, no. 3, pp. 189-197.

• Yamamoto, K., Mizoguti, S., Yoshimitsu, K., and Kawasaki, J. (1983). "Relation between graphitic corrosion and strength-degradation of cast iron pipe", Corrosion Eng., 32(3), 157–162.

Appendix A

Table A 1 shows the tabular values of the stresses and corresponding plastic strains used in the model.

Table A 1: Stresses and plastic strains for non-linear modelling

Stress σ_{tru}	Plastic Strain ε_{pl}
60.18692	0
61.36336	1.93E-06
62.55983	3.97E-06
63.27695	9.20E-06
64.68463	9.84E-06
66.10683	1.04E-05
66.86117	1.54E-05
67.59354	2.05E-05
69.07289	2.06E-05
69.79631	2.58E-05
70.57442	3.07E-05
72.88589	3.53E-05
73.63338	4.03E-05
74.37991	4.53E-05
75.21857	4.97E-05
75.9506	5.49E-05
78.30595	5.92E-05
79.86038	6.89E-05
80.63369	7.37E-05
82.88823	7.87E-05
83.63335	8.37E-05
84.42856	8.85E-05
85.15341	9.36E-05
85.83541	9.91E-05
87.31292	9.93E-05
88.0667	0.000104
88.79238	0.000109
89.51154	0.000115
90.20961	0.00012
91.01373	0.000125
91.78062	0.00013
92.51856	0.000135
94.79946	0.000139
95.55569	0.000144
96.29459	0.000149

97.13037	0.000154
97.80299	0.000159
98.60341	0.000164
99.36108	0.000169
100.1702	0.000174
100.9077	0.000179
101.7284	0.000183
102.45	0.000188
103.2749	0.000193
104.1041	0.000197
104.8722	0.000202
105.6847	0.000207
106.4499	0.000212
107.2461	0.000217
108.0594	0.000221
108.8498	0.000236
109.6317	0.000241
110.4222	0.000245
111.2181	0.00025
112.0271	0.000255
112.8664	0.000259
113.6887	0.000264
114.4846	0.000268
115.2799	0.000273
116.1081	0.000287
116.9048	0.000292
117.7506	0.000297
118.6108	0.000301
119.3849	0.000306
120.2481	0.00031
120.998	0.000325
121.8307	0.000329
122.727	0.000333
123.5089	0.000338
124.3517	0.000353
125.162	0.000357
126.0021	0.000372
126.8279	0.000376
127.7299	0.00038
128.5029	0.000385
129.4223	0.000389
130.2596	0.000403
131.1519	0.000407

131.9808	0.000422
132.8067	0.000426
133.6821	0.00044
134.5074	0.000445
135.3372	0.000459
136.17	0.000464
137.0538	0.000478
137.9041	0.000482
138.7694	0.000496
139.5678	0.000501
140.4351	0.000515
141.3019	0.000529
142.1479	0.000534
143.0094	0.000538
143.9315	0.000552
144.832	0.000566
145.6896	0.00058
146.6035	0.000584
147.4832	0.000598
148.2978	0.000613
149.2693	0.000626
150.1334	0.00063
151.0248	0.000645
151.9744	0.000658
152.8562	0.000672
153.8005	0.000686
154.7441	0.0007
155.6603	0.000714
156.5272	0.000728
157.4352	0.000732
158.3827	0.000755
159.2811	0.000769
160.1734	0.000773
161.0317	0.000788
161.9034	0.000802
162.864	0.000825
163.7526	0.000839
164.6943	0.000843
165.5183	0.000858
166.4133	0.000872
167.3363	0.000895
168.2557	0.000899
169.1591	0.000923

170.1234	0.000937
171.0112	0.000961
171.9461	0.000975
172.9539	0.000988
173.8297	0.001002
174.7704	0.001026
175.7197	0.001049
176.5803	0.001063
177.5292	0.001087
178.4689	0.001111
179.3533	0.001125
180.2573	0.001149
181.1806	0.001173
182.0802	0.001187
183.0157	0.00121
183.9742	0.001234
184.8827	0.001258
185.7666	0.001282
186.679	0.001306
187.6061	0.001329
188.5616	0.001363
189.4761	0.001387
190.3232	0.001411
191.2873	0.001435
192.2356	0.001468
193.1381	0.001492
194.131	0.001515
194.9694	0.00154
195.8696	0.001564
196.8513	0.001597
197.7103	0.001631
198.5732	0.001655
199.4965	0.001689
200.2208	0.001724
201.1349	0.001758
201.9632	0.001792
202.8371	0.001836
203.7019	0.00187
204.5207	0.001905
205.2851	0.00195
206.0943	0.001994
206.9167	0.002028
207.6986	0.002073

208.5128	0.002127
209.3009	0.002162
210.013	0.002217
210.8247	0.002262
211.5675	0.002316
212.2474	0.002372
212.9364	0.002417
213.5411	0.002483